

Multiscale feedback drives viral evolution and epidemic dynamics

Juan C. Muñoz-Sánchez^{1,2,*}, J. Tomás Lázaro^{3,4,5,6,*,+}, Josep Sardanyés^{5,6}, and Santiago F. Elena^{1,7}

¹*Institute for Integrative Systems Biology (I²SysBio), CSIC-Universitat de València, Paterna, 46980 València, Spain*

²*Departament de Física Teòrica, Universitat de València, Burjassot, 46100 València, Spain*

³*Departament de Matemàtiques, Universitat Politècnica de Catalunya (UPC), 08028 Barcelona, Spain*

⁴*Institute of Mathematics, UPC-BarcelonaTech (IMTech), 08028 Barcelona, Spain*

⁵*Centre de Recerca Matemàtica (CRM), Cerdanyola del Vallès, 08193 Barcelona, Spain*

⁶*Dynamical Systems and Computational Virology, CSIC Associated Unit CRM-I²SysBio, Spain*

⁷*Santa Fe Institute, Santa Fe, NM 87501, USA*

^{*}*Equal contribution*

⁺*Correspondence: jose.tomas.lazaro@upc.edu*

January 28, 2026

Abstract

We introduce a minimal multiscale framework that links within-host virus dynamics to population-level SIRS epidemiology through explicit, bidirectional coupling. At the microscopic layer, a two variant quasispecies (master and mutant genomes with packaged virions) evolves on a fast timescale. At the macroscopic layer, two infectious classes (master- and mutant-infected), susceptible, recovered, and deceased individuals evolve slowly. The two scales are connected through transmission rates that depend on instantaneous virion abundance and through prevalence-weighted effective replication rates. Exploiting the timescale separation, we formalize a coarse-grained slow-fast closure: the genome-virion subsystem rapidly relaxes to quasi-steady states that parameterize time-varying transmission in the slow epidemiological system. This yields an integrated expression for the basic reproduction number and sharp inequalities that delineate coexistence *versus* exclusion. A key prediction is a context-dependent error threshold that shifts with the prevalence ratio, enabling transient pseudo-error catastrophes driven by epidemic composition rather than intrinsic fidelity. Linearization reveals parameter regions with damped oscillations arising solely from the microscopic-macroscopic feedback. Two illustrative extremes bracket the model’s behavior: an avirulent strongly immunizing strain that benignly replaces the master, and a hypervirulent weakly immunizing that self-limits via host depletion and collapses transmission. This framework yields testable signatures linking viral load, incidence, and within-host composition.

1 Introduction

Viruses infect every form of life, from viruses and microbes to plants and animals. Most coexist with their hosts, but spillovers into new hosts can cause disease and reduce host fitness. At the same time, viruses can drive host innovations (*e.g.*, [1, 2]). Viral biology is studied across multiple scales: molecular virologists dissect replication, pathogenesis, and antiviral defenses within cells; clinicians focus on individuals; and ecologists and epidemiologists track incidence, transmission, and ecosystem-level impacts. Accordingly, what constitutes the “host” (cell or tissue, individual or population and ecosystem) and the operative “viral unit” (mutant swarms within individuals, infected hosts in ecological studies, or evolutionary lineages in phylogeography) shifts with scale. Yet the ultimate host is the cell, where viral genes are expressed, replication organelles form, genomes and proteins are synthesized, host defenses are countered, particles assemble, and infection spreads to neighboring cells, tissues, new hosts, and ultimately through populations and ecosystems. Selective pressures

also differ across scales: rapid replication may confer an advantage within hosts but prove suboptimal for between-host transmission [3]. Thus, although the qualitative link between within-host infection dynamics and population-level transmission is widely acknowledged, a comprehensive, quantitative framework that integrates these scales remains lacking.

As complex dynamical systems, viruses can exhibit phase transitions involving abrupt changes in dynamical behavior or internal structure [4]. At the molecular level, critical phenomena are exemplified by the error threshold associated to highly mutagenic replication of viral genomes [5, 6]. At the epidemiological level, the spread of viral diseases across heterogeneous contact networks displays complex dynamical behavior and phase transitions associated with the existence of highly connected hubs [7, 8]. So far, models connecting phase transitions across biological scales deserve further exploration. In particular, no comprehensive framework has yet been developed to investigate whether transitions at one level may result from the dynamical properties of the lower levels.

There have been few attempts to model multiscale selection in viruses. Existing studies have treated between-host transmissions as a function of within-host replication parameters [9–15], or tissue and organ colonization as an extension of within-cell replication processes and their interaction with host factors [16–18]. Unfortunately, the former models usually neglect the inherent within-host complexity, while the latter rarely extend beyond individual tissues or single hosts. Modeling multiscale processes in full mechanistic detail is therefore unrealistic. One alternative is to extract the essential features of lower-scale models to embed them into higher-scale descriptions [10]. An approach that has been successfully taken is to separate timescales, which enables the construction of effective reduced models that operate at distinct biological scales.

Predicting when a viral mutant genotype will rise to dominance and potentially trigger an epidemic is a critical challenge. This problem inherently involves two scales: a microscopic scale, at which a mutant genome is generated from a master sequence, and a macroscopic, or population scale, at which the new virus must sustain a transmission chain to remain in circulation and outcompete existing strains. At the microscopic level, quasispecies theory provides a dynamical framework for replicator evolution under mutation–selection balance and predicts the existence of an error threshold, beyond which genetic information cannot be stably maintained [5, 6]. This threshold has been experimentally identified in RNA viruses [19] and has been proposed to operate in hepatitis C virus-infected patients through replicative, rather than mutational, thresholds [20]. At the population level, a range of epidemiological models describes viral transmission in terms of biologically meaningful parameters, with the Susceptible-Infectious-Recovered (SIR) model and its variants being among the most fundamental.

In this work, we propose a multiscale modelling approach that integrates known intracellular replication dynamics with macroscopic population-level transmission. Our objective is to better understand the characteristics a mutant virus must possess to become dominant, potentially replacing the master sequence entirely. The link between both scales has been explicitly made by expressing the macroscopic transmission rates as a function of the number of viral particles produced in infected cells. In addition, we explore how population level processes can drive the extinction of specific viral strains and how intracellular dynamics can trigger nontrivial epidemic events.

Among our findings, we present a formulation for the basic reproduction number, \mathcal{R}_0 , that incorporates parameters from both scales, thereby providing a more comprehensive measure of viral fitness. Among the many scenarios that can be analyzed within our framework, we illustrate two extremes along a continuum: an avirulent virus with rapid recovery that induces temporal immunity (*i.e.*, a vaccine-like virus) and a hypervirulent virus with slow recovery (*i.e.*, a burnout virus). In the first scenario, the master sequence is replaced by the avirulent mutant, which persists at a high incidence in the host population. In the second scenario, all infected individuals eventually die, extinguishing the infection, leaving only susceptible individuals in the population.

Understanding variant emergence and competition requires an integrated multiscale view. At the intracellular level, viruses form quasispecies —mutant swarms generated by high replication error rates— while at the population level, compartmental models (*e.g.*, SIR) capture spread among hosts. These scales are deeply interconnected: evolutionary pressures depend on macroscopic factors (population immunity, transmission opportunities), and a variant’s success hinges on both between-host transmissibility (macroscopic) and within-host replicative fitness (microscopic). The COVID-19 pandemic illustrates this coupling, with co-circulating SARS-CoV-2 variants adapting via random mutation under biological and social/behavioral selection pressures [21].

2 Multiscale mathematical model

We propose a minimal multiscale model that links within-host and population dynamics: a quasispecies module describing mutation from a master to a single dominant mutant genome within an average host is coupled to a two-strain SIRS system that distinguishes individuals infected by each variant. For analytical clarity, mutation is assumed to be unidirectional (no reverse mutation or lineage diversification). This is a common assumption in quasispecies models: the probability of backward mutations is extremely low due to the enormous size of the sequence space [22]. The model comprises two layers and two time scales (Figure 1): a fast microscopic layer tracking genome and virion abundances for the master (g_0, v_0) and for the averaged mutant (g_1, v_1), and a slow macroscopic SIRS layer with infectious classes I_0 and I_1 ; no inflow of susceptible individuals is included. The layers are bidirectionally coupled: transmission rates in the SIRS module depend on the virion distribution, while key microscopic parameters are modulated by the current epidemiological state. Despite its idealization, this framework captures the emergence, competition, and replacement of dominant variants and clarifies conditions that favor the rise of new strains. The detailed models at each level are:

- **Microscopic level.** At the genome's level the model follows a variant of the Swetina-Schuster quasispecies approach [23]:

$$\varepsilon \dot{g}_0 = f_0(1 - \mu)\nu_0 g_0 - \Phi g_0, \quad (1)$$

$$\varepsilon \dot{g}_1 = f_0\mu\nu_0 g_0 + f_1\nu_1 g_1 - \Phi g_1, \quad (2)$$

where g_0 and g_1 are the master and the pool of mutant genomes, respectively, $f_0 > f_1 > 0$ are their fitness rates, and $0 \leq \mu \leq 1$ is the mutation probability. The parameter $\varepsilon > 0$ is assumed to be small. Moreover, being I_0 and I_1 the prevalence of two different types of infectious individuals, we denote by

$$\nu_0 = \nu_0(I_0, I_1) = \frac{I_0}{I_0 + I_1} \quad \text{and} \quad \nu_1 = \nu_1(I_0, I_1) = \frac{I_1}{I_0 + I_1} \quad \text{if } (I_0, I_1) \neq (0, 0), \quad (3)$$

and 0 otherwise, the relative prevalence of I_i with respect to the total infected individuals $I_0 + I_1$. Since, in our case, all the infectious individuals arise from these two types, it follows that $\nu_1 = 1 - \nu_0$, except when $I_0 = I_1 = 0$, in which $\nu_0 = \nu_1 = 0$.

The function Φ in (1)-(2) is the standard outflow term introduced to keep the total population of genomes, $g_0 + g_1$, constant. In this scenario this is given by

$$\Phi = f_0\nu_0 \frac{g_0}{g_0 + g_1} + f_1\nu_1 \frac{g_1}{g_0 + g_1}.$$

If we take g_0, g_1 such that $g_0(0) + g_1(0) = 1$ (so, we will talk about frequencies) this function becomes

$$\Phi = f_0\nu_0 g_0 + f_1\nu_1 g_1$$

and hence $g_0(t) + g_1(t) = 1 \forall t \geq 0$. This will be assumed along this work. Whenever both infected populations I_0, I_1 simultaneously vanish (total virus extinction), the system (1)-(2) becomes $\varepsilon \dot{g}_0 = 0$, $\varepsilon \dot{g}_1 = 0$.

It is well-known in quasispecies theory, the existence of the so-called critical mutation driving the system into error catastrophe, a value for μ beyond which the master sequence disappears and only mutants persist [4–6]. In our case, it is given ¹ by

$$\mu_c = 1 - \frac{f_1}{f_0} \left(\frac{1}{\nu_0} - 1 \right), \quad (4)$$

only defined for $I_0 > 0$ (otherwise g_0 cannot replicate). The terms ν_0 and ν_1 connect the microscopic to the macroscopic layers by incorporating the assumption that infected individuals become a necessary substrate for the replication of viral genomes. The fitness rates are modulated by the fraction of infected individuals of each type.

¹It suffices to define the effective fitnesses $\tilde{f}_0 = f_0\nu_0$ and $\tilde{f}_1 = f_1\nu_1 = f_1(1 - \nu_0)$ and to use the classical formula $\mu_c = 1 - \tilde{f}_1/\tilde{f}_0$.

Concerning the virion's layer, we consider

$$\varepsilon \dot{v}_0 = \xi_0 g_0 - \gamma_0 v_0, \quad (5)$$

$$\varepsilon \dot{v}_1 = \xi_1 g_1 - \gamma_1 v_1, \quad (6)$$

where v_0 and v_1 are the corresponding virions for the genomes g_0 and g_1 , respectively, $\xi_{0,1} > 0$ denote their encapsidation constants, and $\gamma_{0,1} > 0$ their degradation rates.

Notice, for the genome's and virion's systems, the inclusion of the small parameter $\varepsilon > 0$ which makes the microscopic level to evolve much faster in time than its counterpart macroscopic one (see below). This leads to a two-timescales model.

- **Macroscopic level.** This is defined as a SIRS epidemiological model with feedback with the microscopic layer. The variables S stands for susceptible individuals, I_j for infectious (and infected) by virions' type v_j ($j = 0, 1$), R for recovered and D for dead. Precisely, this model reads

$$\dot{S} = -(\beta_{00} I_0 + \beta_{01} I_0 + \beta_{11} I_1) S + \chi R, \quad (7)$$

$$\dot{I}_0 = \beta_{00} I_0 S - (\pi_0 + \delta_0) I_0, \quad (8)$$

$$\dot{I}_1 = (\beta_{01} I_0 + \beta_{11} I_1) S - (\pi_1 + \delta_1) I_1, \quad (9)$$

$$\dot{R} = \pi_0 I_0 + \pi_1 I_1 - \chi R, \quad (10)$$

$$\dot{D} = \delta_0 I_0 + \delta_1 I_1 \quad (11)$$

where $\delta_{0,1}$ denote the viral-induced mortality rates, $\pi_{0,1}$ the recovery rates, and the virions' dependent infection rates $\beta_{00}, \beta_{01}, \beta_{11}$ that will connect the micro- and macroscopic levels (see below). The parameter $\chi > 0$ is the waning immunity rate; it is assumed (for simplicity) to be the same for both type of viruses (master and its mutant). The no-presence of the small parameter ε makes this macroscopic system slow in comparison with the microscopic level.

Observe that $\dot{S} + \dot{I}_0 + \dot{I}_1 + \dot{R} + \dot{D} = 0$ and so $S(t) + I_0(t) + I_1(t) + R(t) + D(t)$ is a first integral of the system (7)-(11). This implies that $S(t) + I_0(t) + I_1(t) + R(t) + D(t) = S(0) + I_0(0) + I_1(0) + R(0) + D(0)$ for any $t \geq 0$. It is not a loss of generality to assume this value equal to 1 and so consider the variables S, I_0, I_1, R , and D to represent fractions of the total (invariant) population.

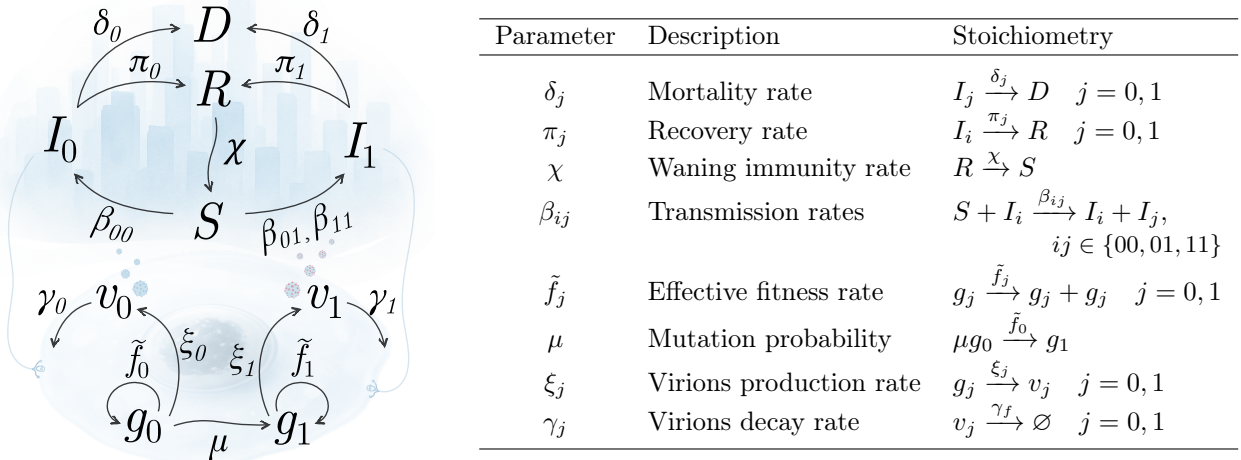


Figure 1: Schematic representation of the multiscale model (left) and summary of the associated parameters (right). Microscopic variables include the master and mutated genomes (g_0, g_1) and their corresponding virions (v_0, v_1), while macroscopic variables comprise susceptible (S), infected (I_0, I_1), recovered (R), and deceased (D) individuals.

2.1 Multiscale coupling between microscopic and macroscopic dynamics

The coupling between microscopic and macroscopic levels in our model arises through the construction of key parameters that bridge the two scales. We propose the following bidirectional connections:

1. **From microscopic to macroscopic dynamics via transmission rates.** A connection from the intra-host to the population level is established through the transmission rates, denoted by $\beta_{ij}(v_j(t))$. These rates quantify the efficiency with which an individual infected with variant i transmits the infection to a susceptible individual, who subsequently develops an infection caused by variant j . Crucially, we assume that these rates depend on the instantaneous concentration of virions, $v_j(t)$, associated with each viral variant ². This dependence is modeled using a hyperbolic-like function, which captures the saturating nature of transmission dynamics with increasing viral load.

To account for the different infection pathways, we define three ³ distinct transmission rates:

- $\beta_{00}(v_0)$: transmission from a master-infected individual leading to a new master infection.
- $\beta_{01}(v_1)$: transmission from a master-infected individual leading to a new mutant infection.
- $\beta_{11}(v_1)$: transmission from a mutant-infected individual leading to a new mutant infection.

To estimate the effective availability of mutant virions v_1 within the population, we assume a proportional distribution of v_1 between the two types of infected individuals. Specifically, we define:

$$v_1^{(j)} = v_1 \cdot \frac{I_j}{I_0 + I_1} = v_1 \nu_j$$

This assumption reflects the idea that the total mutant viral load is partitioned among infected individuals proportionally to their prevalence. Furthermore, these expressions then inform the variant-specific transmission terms used in the population-level model.

The transmission rates are assumed to follow a saturation function of the form:

$$\beta_{00} = \beta_{00}(v_0) = \frac{a_0 v_0}{b_0 + v_0}, \quad \beta_{01} = \beta_{01}(v_1) = \frac{a_1 \nu_0 v_1}{b_1 + \nu_0 v_1}, \quad \beta_{11} = \beta_{11}(v_1) = \frac{a_1 \nu_1 v_1}{b_1 + \nu_1 v_1} = \frac{a_1 (1 - \nu_0) v_1}{b_1 + (1 - \nu_0) v_1},$$

with constants $a_{0,1} \geq 0$, $b_{0,1} > 0$, and $\nu_0 = \nu(I_0, I_1)$ as defined in (3). Biologically, $a_{0,1}$ represents the contagion potential (*i.e.*, the maximum value of the transmission rate function), and $b_{0,1}$ represents the characteristic viral load at which the contagion rate reaches half of its maximal value. The terms $\nu_0 v_1$ and $\nu_1 v_1$ in β_{01}, β_{11} represent the fractions of mutant virions produced within master-infected individuals and mutant-infected individuals, respectively.

2. **Macroscopic to microscopic levels via prevalence.** Conversely, to represent how population-level dynamics influence viral evolution at the intracellular scale, we modulate the replicative fitness of each variant based on the relative abundance of host types in the population. Since infected individuals act as the primary replication environment for the virus, the availability of hosts directly affects the success of the variants. Although mutant virions may replicate to some extent in individuals originally infected with the master variant, for simplicity, we assume that each viral variant replicates predominantly within its corresponding host type. Thus, the replicative fitness parameters are defined as functions of the current population state:

$$\tilde{f}_0(t) = f_0 \cdot \frac{I_0(t)}{I_0(t) + I_1(t)} = \nu_0(t) f_0, \quad \tilde{f}_1(t) = f_1 \cdot \frac{I_1(t)}{I_0(t) + I_1(t)} = \nu_1(t) f_1 = (1 - \nu_0(t)) f_1,$$

where f_0 and f_1 are the baseline fitness values for the master and mutant variants, respectively. These bidirectional links enable the model to capture feedback loops between within-host dynamics and between-host transmission, offering insights into how selective pressures at one scale shape dynamics at the other.

²Recall that within I_0 individuals, g_0 replicates generating g_1 . Therefore, both virion types can be produced. In contrast, within I_1 individuals only g_1 replicates, given our assumption of no back mutation.

³Notice that $\beta_{10} = 0$, since mutant-infected individuals (I_1) do not carry master virions, $v_0^{(1)} = 0$, and thus cannot generate new infections of the master type.

It is important to note that, in this framework, the term “multiscale” refers not only to interactions between biological levels (intracellular and population) but also to the separation of time scales between them. Specifically, we assume that microscopic (within-host) dynamics occur on a much faster timescale than macroscopic (population-level) dynamics.

Regarding notation, from this point onward we denote $\nu = \nu_0$ and, consequently, $\nu_1 = 1 - \nu_0 = 1 - \nu$. This convention fails only in the special case $I_0 = I_1 = 0$, for which $\nu_0 = \nu_1 = 0$. This case is explicitly addressed at the appropriate point in the analysis.

3 Results and discussion

3.1 Equilibrium points

We begin by computing the equilibrium points of systems (1)-(2), (5)-(6) and (7)-(11). Together with other invariant objects, these equilibria constitute the dynamical skeleton of the system and fully determine its dynamics. Henceforth, we assume that the virions encapsidation and degradation rates are positive, *i.e.* $\xi_{0,1} > 0$ and $\gamma_{0,1} > 0$, and that $\mu \in (0, 1]$ (*i.e.*, there is always g_1 production due to errors in g_0 replication).

The different classes of equilibrium points are classified according to the type (if any) of infected individuals that remain:

- **DFE**: disease-free equilibrium, when $I_0 = I_1 = 0$.
- **NME**: equilibrium with no master-infected individuals, $I_0 = 0, I_1 > 0$.
- **NmutE**: equilibrium with no mutant-infected individuals, $I_0 > 0$ and $I_1 = 0$;
- **CSE**: co-circulating strains equilibrium, with $I_0 > 0, I_1 > 0$.

The explicit expressions of such equilibria are provided in the following propositions. To ease the reading, their proofs have been deferred to Appendix A.

We also impose the following assumptions on model parameters to restrict the range of feasible scenarios:

- **Microscopic system**: $\mu \in (0, 1]$ and $f_0 > f_1 > 0$ (genomes); $\xi_{0,1} \geq 0$ and $\gamma_{0,1} > 0$ (virions).
- **Macroscopic system**: $a_{0,1} \geq 0, b_{0,1} > 0, \delta_{0,1} \geq 0, \pi_{0,1} \geq 0$, and $\chi \geq 0$ (individuals).

Let us start with a result showing the close connection between microscopic and macroscopic equilibrium points through the relative prevalence $\nu(I_0, I_1)$ and the critical mutation probability μ_c .

Lemma 1 (macroscopic to microscopic equilibrium points) *Let us assume that (I_0^*, I_1^*) , both positive, are the I -variables of an equilibrium point for the macroscopic system (7)-(11), and denote $\nu^* = \nu_0^* = \nu(I_0^*, I_1^*) \in (0, 1)$, as defined in (3), the relative prevalence of I_0^* with respect to $I_0^* + I_1^*$. Assume that the microscopic system (1)-(6) has given parameters $\mu \in (0, 1]$, $f_0 > f_1 > 0$, $\xi_{0,1} \geq 0$, and $\gamma_{0,1} > 0$.*

Let us define new fitnesses $\tilde{f}_0^ = f_0\nu^*$ and $\tilde{f}_1^* = f_1(1 - \nu^*)$ and consider the associated quasispecies system. Denote by μ_c^* its corresponding critical mutation probability at equilibrium*

$$\mu_c^* = 1 - \frac{f_1}{f_0} \left(\frac{1}{\nu^*} - 1 \right),$$

for $\nu^* > 0$. Then, the equilibrium points for the genome-virion system associated to the I -equilibrium values I_0^* , I_1^* , have the following expression:

$$\begin{aligned} \text{QS}_{\text{mic}}^{(\mu_c^*)} : \quad (g_0^*, g_1^*; v_0^*, v_1^*) &= \left(1 - \frac{\mu}{\mu_c^*}, \frac{\mu}{\mu_c^*}; \frac{\xi_0}{\gamma_0} g_0^*, \frac{\xi_1}{\gamma_1} g_1^*\right) && \text{if } 0 < \mu < \mu_c^* \\ (g_0^*, g_1^*; v_0^*, v_1^*) &= \left(0, 1; 0, \frac{\xi_1}{\gamma_1}\right) && \text{if } \mu_c^* \leq \mu \leq 1, \end{aligned}$$

Proposition 1 (disease-free equilibrium (DFE) points) Let us assume an equilibrium point satisfying that $I_0^* = I_1^* = 0$. Then, the microscopic equilibrium variables are of the form:

$$\text{QS}_{\text{mic}} : (g_0, g_1, v_0, v_1) = \left(g_0, 1 - g_0, \frac{\xi_0}{\gamma_0} g_0, \frac{\xi_1}{\gamma_1} (1 - g_0)\right),$$

for arbitrary g_0, g_1 such that $g_0 + g_1 = 1$. Regarding the complete equilibrium point, two cases arise:

(i) If the waning immunity rate satisfies $\chi > 0$, the equilibrium must take the form:

$$(S, I_0^*, I_1^*, R^*, D) \times (g_0, g_1; v_0, v_1) = (S, 0, 0, 0, D) \times \{\text{QS}_{\text{mic}}\},$$

with arbitrary S, D such that $S + D = 1$.

(ii) If instead the waning immunity rate vanishes, $\chi = 0$, it is given by:

$$(S, I_0^*, I_1^*, R, D) \times (g_0, g_1; v_0, v_1) = (S, 0, 0, R, D) \times \{\text{QS}_{\text{mic}}\},$$

with arbitrary S, R, D such that $S + R + D = 1$.

Proposition 2 (no master equilibrium (NME) points) Equilibrium points with no master-infected individuals and surviving mutant-infected individuals, i.e. $I_0^* = 0, I_1^* > 0$, exist if and only if $\delta_1 = 0$.

Moreover, the microscopic system at equilibrium falls into one of the following two cases:

$$\text{QS}_{\text{mic}}^{(0)} : (g_0^*, g_1^*, v_0^*, v_1^*) = \left(1, 0, \frac{\xi_0}{\gamma_0}, 0\right) \quad \text{or} \quad \text{QS}_{\text{mic}}^{(1)} : (g_0^*, g_1^*, v_0^*, v_1^*) = \left(0, 1, 0, \frac{\xi_1}{\gamma_1}\right).$$

The complete equilibrium must therefore belong to one of these cases:

(i) Case $\chi > 0$.

(i₁) Case $\beta_{11} > 0$:

$$(S^*, I_0^*, I_1^*, R^*, D^*) \times (g_0^*, g_1^*; v_0^*, v_1^*) = \left(\frac{\pi_1}{\beta_{11}}, 0, I_1^*, \frac{\pi_1}{\chi} I_1, D^*\right) \times \left\{\text{QS}_{\text{mic}}^{(0)}, \text{QS}_{\text{mic}}^{(1)}\right\},$$

such that $\frac{\pi_1}{\beta_{11}^*} + I_1^* \left(1 + \frac{\pi_1}{\chi}\right) + D^* = 1$.

(i₂) Case $\beta_{11} = 0$: then, necessarily, $\pi_1 = 0$, and

$$(S, I_0^*, I_1^*, R^*, D) \times (g_0^*, g_1^*; v_0^*, v_1^*) = (S, 0, I_1^*, 0, D) \times \left\{\text{QS}_{\text{mic}}^{(0)}, \text{QS}_{\text{mic}}^{(1)} \text{ iff } a_1 = 0 \text{ or } \xi_1 = 0\right\},$$

with arbitrary S and D such that $S + I_1^* + D = 1$.

(ii) Case $\chi = 0$:

(ii₁) Case $\beta_{11} > 0$: then, necessarily, $\pi_1 = 0$ and

$$(S^*, I_0^*, I_1^*, R, D) \times (g_0^*, g_1^*; v_0^*, v_1^*) = (0, 0, I_1^*, R, D) \times \left\{\text{QS}_{\text{mic}}^{(0)}, \text{QS}_{\text{mic}}^{(1)}\right\},$$

with arbitrary R and D such that $I_1^* + R + D = 1$.

(ii₂) Case $\beta_{11} = 0$: then, as above, it follows that $\pi_1 = 0$, and hence,

$$(S, I_0^*, I_1^*, R, D) \times (g_0^*, g_1^*; v_0^*, v_1^*) = (S, 0, I_1, R, D) \times \left\{ \text{QS}_{\text{mic}}^{(0)}, \text{QS}_{\text{mic}}^{(1)} \text{ iff } a_1 = 0 \text{ or } \xi_1 = 0 \right\},$$

with arbitrary S , R , and D satisfying that $S + I_1^* + R + D = 1$.

Proposition 3 (no mutant equilibrium (NmutE) points) *An equilibrium point exists with no mutant-infected individuals and survival master-infected individuals, i.e. $I_0^* > 0, I_1^* = 0$, if and only if $\delta_0 = 0$. If so, the corresponding equilibria for the microscopic system are of the form, either*

$$\text{QS}_{\text{mic}}^{(1)} : (g_0^*, g_1^*; v_0^*, v_1^*) = \left(0, 1, 0, \frac{\xi_1}{\gamma_1} \right),$$

or

$$\text{QS}_{\text{mic}}^{(\mu)} : (g_0^*, g_1^*; v_0^*, v_1^*) = \left(1 - \mu, \mu, \frac{\xi_0}{\gamma_0}(1 - \mu), \frac{\xi_1}{\gamma_1}\mu \right), \quad 0 < \mu < 1.$$

Regarding the equilibria of the macroscopic system, they must belong to one of the following cases:

(i) Case $\chi > 0$. It results in four different scenarios according to the value of β_{00} and β_{01} :

(i₁) Case $\beta_{00} = 0$ and $\beta_{01} > 0$. It follows that $\pi_0 = 0$ and the macroscopic equilibrium point is

$$(S^*, I_0^*, I_1^*, R^*, D^*) = (0, I_0^*, 0, 0, 1 - I_0^*).$$

(i₂) Case $\beta_{00} > 0$ and $\beta_{01} = 0$. The macroscopic equilibrium reads

$$(S^*, I_0^*, I_1^*, R^*, D^*) = \left(\frac{\pi_0}{\beta_{00}}, I_0^*, 0, \frac{\pi_0}{\chi} I_0^*, 1 - \frac{\pi_0}{\beta_{00}} - I_0^* \left(1 + \frac{\pi_0}{\chi} \right) \right),$$

$$\text{with } 0 < I_0^* \leq \frac{1 - \pi_0/\beta_{00}}{1 + \pi_0/\chi}.$$

(i₃) Case $\beta_{00} > 0$ and $\beta_{01} > 0$. It follows that $\pi_0 = 0$ and the macroscopic equilibrium is

$$(S^*, I_0^*, I_1^*, R^*, D^*) = (0, I_0^*, 0, 0, 1 - I_0^*).$$

(i₄) Case $\beta_{00} = 0$ and $\beta_{01} = 0$. Here $\pi_0 = 0$ and the macroscopic equilibrium has the expression

$$(S, I_0^*, I_1^*, R, D) = (S, I_0^*, 0, 0, D),$$

with S , I_0^* and D such that $S + I_0^* + D = 1$.

(ii) Case $\chi = 0$. It implies that $\pi_0 = 0$. This, in its turn, is also conveniently divided into four cases, as their microscopic states at equilibrium might differ:

(ii₁) Case $\beta_{00} = 0$ and $\beta_{01} > 0$. The macroscopic equilibrium point is given by

$$(S^*, I_0^*, I_1^*, R, D) = (0, I_0^*, 0, R, D),$$

with I_0^* , R and D such that $I_0^* + R + D = 1$.

(ii₂) Case $\beta_{00} > 0$ and $\beta_{01} = 0$. The macroscopic equilibrium reads

$$(S^*, I_0^*, I_1^*, R, D) = (0, I_0^*, 0, R, D),$$

with I_0^* , R and D such that $I_0^* + R + D = 1$.

(ii₃) Case $\beta_{00} > 0$ and $\beta_{01} > 0$. Here, the macroscopic equilibrium is

$$(S^*, I_0^*, I_1^*, R, D) = (0, I_0^*, 0, R, D),$$

with I_0^* , R and D such that $I_0^* + R + D = 1$.

(ii₄) Case $\beta_{00} = 0$ and $\beta_{01} = 0$. Here, the equilibrium has the expression

$$(S, I_0^*, I_1^*, R, D) = (S, I_0^*, 0, R, D).$$

with S , I_0^* , R and D such that $S + I_0^* + R + D = 1$.

The full equilibrium state emerges from the coupling between the macroscopic and microscopic equilibria characterized above. To avoid confusion and maintain clarity, we leave the explicit construction of the combined equilibrium to the reader. The number of admissible configurations can be substantially reduced by fixing certain parameters in advance. Nevertheless, the construction of both the microscopic and macroscopic equilibria is subject to mutual constraints; each imposes compatibility conditions on the other that must be accounted for in the analysis. These constraints depend on the value of β_{00} and β_{01} as follows:

- (i) If $\beta_{00} = 0$ then either $a_0 = 0$ or $v_0^* = 0$. The latter may occur either because $\xi_0 = 0$ or $g_0^* = 0$, which in turn implies $\mu = 1$ in the microscopic equilibrium $QS_{\text{mic}}^{(\mu)}$.
- (ii) If $\beta_{01} = 0$ then either $a_1 = 0$ or $v_1^* = 0$. The second case implies either $\xi_1 = 0$ or $g_1^* = 0$, which is only possible in the extreme case $\mu = 0$ (see Sec. 3.5).
- (iii) For $\beta_{00} > 0$ to hold, it is necessary that $v_0^* > 0$, which is incompatible with the microscopic state $QS_{\text{mic}}^{(1)}$.

Proposition 4 (Co-circulating strains equilibrium (CSE) points) Let consider a co-circulating strains equilibrium point, i.e. $I_0^* > 0$ and $I_1^* > 0$. Then, necessarily, $\delta_0 = \delta_1 = 0$. If so, the corresponding equilibria for the microscopic system are of the form:

$$\begin{aligned} QS_{\text{mic}}^{(\mu_c^*)} : \quad (g_0^*, g_1^*; v_0^*, v_1^*) &= \left(1 - \frac{\mu}{\mu_c^*}, \frac{\mu}{\mu_c^*}; \frac{\xi_0}{\gamma_0} g_0^*, \frac{\xi_1}{\gamma_1} g_1^* \right) && \text{if } 0 < \mu < \mu_c^* \\ (g_0^*, g_1^*; v_0^*, v_1^*) &= \left(0, 1; 0, \frac{\xi_1}{\gamma_1} \right) && \text{if } \mu_c^* \leq \mu \leq 1, \end{aligned}$$

where

$$\mu_c^* = 1 - \frac{f_1}{f_0} \left(\frac{1}{\nu^*} - 1 \right).$$

It follows that the infection rates β_{01} and β_{11} either vanish simultaneously or are both nonzero. Consequently, the complete macroscopic and microscopic equilibria must fall into one of the following cases:

- (i) Case $\chi > 0$.

With two cases, according to the value of the master infection rate β_{00} :

- (i₁) Case $\beta_{00} = 0$.

In this case, necessarily, the master recovery rate must vanish: $\pi_0 = 0$. Moreover we have:

- (a) Case $\beta_{01} > 0, \beta_{11} > 0$.

They equilibrium are of the form

$$(S^*, I_0^*, I_1^*, R^*, D) \times (g_0^*, g_1^*; v_0^*, v_1^*) = \left(\frac{\pi_1 I_1^*}{\beta_{01}^* I_0^* + \beta_{11}^* I_1^*}, I_0^*, I_1^*, \frac{\pi_1}{\chi} I_1^*, D^* \right) \times QS_{\text{mic}}^{(\mu_c^*)},$$

where $S^* + I_0^* + I_1^* + R^* + D^* = 1$.

- (b) Case $\beta_{01} = \beta_{11} = 0$.

Necessarily, no mutant recovery rate, $\pi_1 = 0$, and the equilibrium points are of type

$$(S, I_0^*, I_1^*, R, D) \times (g_0^*, g_1^*; v_0^*, v_1^*) = (S, I_0^*, I_1^*, 0, D) \times QS_{\text{mic}}^{(\mu_c^*)},$$

with arbitrary S , D such that $S + I_0^* + I_1^* + D = 1$ and provided $QS_{\text{mic}}^{(\mu_c^*)}$ satisfies $\beta_{01}^* = \beta_{11}^* = 0$.

(i₂) Case $\beta_{00} > 0$.

If the condition

$$\pi_1 > \frac{\beta_{11}}{\beta_{00}} \pi_0$$

holds, the equilibrium points are of the form

$$(S, I_0^*, I_1^*, R, D) \times (g_0^*, g_1^*; v_0^*, v_1^*) = \left(\frac{\pi_0}{\beta_{00}^*}, I_0^*, \frac{\beta_{01}^* \pi_0}{\beta_{00}^* \pi_1 - \beta_{11}^* \pi_0} I_0^*, \frac{1}{\chi} \left(\pi_0 + \pi_1 \frac{\beta_{01}^* \pi_0}{\beta_{00}^* \pi_1 - \beta_{11}^* \pi_0} \right) I_0^*, D^* \right) \times \text{QS}_{\text{mic}}^{(\mu_c^*)}$$

Moreover, one has that $\beta_{01}^* > 0$ and $\beta_{11}^* > 0$.

(ii) Case $\chi = 0$.

Necessarily, $\pi_0 = \pi_1 = 0$ must hold. Then, we have:

(ii₁) Case $\beta_{00} = 0$.

We distinguish two possible situations:

(a) Case $\beta_{01} > 0, \beta_{11} > 0$.

Here, the equilibria are of type:

$$(S^*, I_0^*, I_1^*, R, D) \times (g_0^*, g_1^*; v_0^*, v_1^*) = (0, I_0^*, I_1^*, R, D) \times \text{QS}_{\text{mic}}^{(\mu_c^*)},$$

with arbitrary R, D such that $I_0^* + I_1^* + R + D = 1$ and provided $\text{QS}_{\text{mic}}^{(\mu_c^*)}$ is compatible with $\beta_{00} = 0$.

(b) Case $\beta_{01} = \beta_{11} = 0$.

In this scenario, we have that S, R , and D are arbitrary. So, the complete equilibrium is of the form

$$(S, I_0^*, I_1^*, R, D) \times (g_0^*, g_1^*; v_0^*, v_1^*) = (S, I_0^*, I_1^*, R, D) \times \text{QS}_{\text{mic}}^{(\mu_c^*)},$$

with $S + I_0^* + I_1^* + R + D = 1$ and provided $\text{QS}_{\text{mic}}^{(\mu_c^*)}$ is compatible with the conditions $\beta_{01} = \beta_{11} = 0$.

(ii₂) Case $\beta_{00} > 0$.

$$(S^*, I_0^*, I_1^*, R, D) \times (g_0^*, g_1^*; v_0^*, v_1^*) = (0, I_0^*, I_1^*, R, D) \times \text{QS}_{\text{mic}}^{(\mu_c^*)},$$

with arbitrary R , and D such that $I_0^* + I_1^* + R + D = 1$

Remark 1 It is easy to see, from equation $\dot{D} = \delta_0 I_0 + \delta_1 I_1$, that the only possible scenario admitting - if any - periodic solutions is when both strains (master and mutant) do not induce mortality. Indeed, $\dot{D} > 0$ and so D increases unless $\delta_0 = \delta_1 = 0$. It can be an interesting point to study but it is out of the scope of this work.

Figure 2 provides a schematic representation of the system's equilibrium structure as a function of the parameters $\beta_{00}, \beta_{01}, \beta_{11}$, and χ . Lines, planes and prisms are labeled with the corresponding equilibrium point form they give rise to. Dashed lines mean "open" in the space of parameters (i.e., they do not include the boundary).

3.2 Computation of the basic reproduction number \mathcal{R}_0

The basic reproduction number \mathcal{R}_0 is a threshold quantity that measures the potential for the spread of an infectious disease. It is usually defined as the average number of secondary infections generated by a single infectious individual introduced into a fully susceptible population (see [24] and references therein). The computation of \mathcal{R}_0 provides an equivalent criterion, in terms of the parameters of the model, for determining the local stability of the DFE prior to the introduction of the first infectious individual. In our model (7)–(11), the DFE corresponds to the state

$$(S, I_0, I_1, R, D) = (S(0), 0, 0, 0, 0) = (1, 0, 0, 0, 0),$$

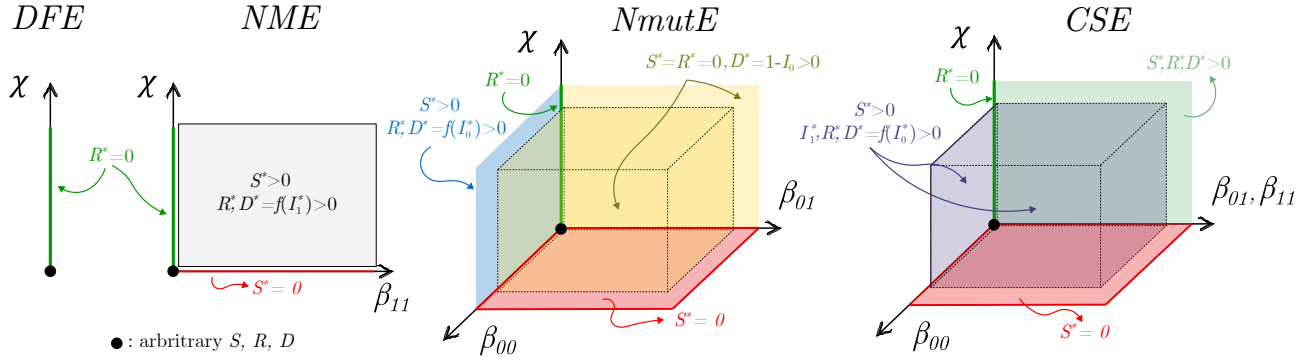


Figure 2: Schematic representation of the four different equilibrium points (DFE, NME, NmutE, and CSE) in terms of the parameters β_{00} , β_{01} , β_{11} , and χ . Dashed lines represent open faces of the prism not included in the corresponding domain. The black dot indicates the origin.

in which the population consists entirely of susceptible individuals (with no recovered or deceased individuals, as the disease has not yet emerged).

Its local stability can be analyzed by linearizing the system around this equilibrium and computing the corresponding eigenvalue spectrum. Specifically: (i) if all the eigenvalues of its jacobian matrix have negative real part, the DFE is locally asymptotically stable; the introduction of an infectious individual, interpreted as a small perturbation, the disease does not spread. (ii) Conversely, if there exists some eigenvalue with positive real part, the DFE is unstable. The introduction of an infectious individual now leads to epidemic outbreak.

A standard method to compute \mathcal{R}_0 is based on the Next Generation Matrix (NGM), introduced in [25]. The NGM method we use in this work is based on [26, 27]. To this end, we split the variables (S, I_0, I_1, R, D) into two compartments: the disease compartment $x = (I_0, I_1)$, and the disease-free compartment $y = (S, R, D)$. We then write the original system in the form

$$\dot{x}_i = \mathcal{F}_i(x, y) - \mathcal{V}_i(x, y) \quad i = 1, \dots, n, \quad \dot{y}_j = g_j(x, y), \quad j = 1, \dots, m, \quad (12)$$

where \mathcal{F}_i denotes the inflow of new infections in compartment i , and \mathcal{V}_i the rate of transmissions between compartment i and other infected compartments. As noted explicitly in [27], the decomposition into \mathcal{F} and \mathcal{V} is not unique and depends on the biological interpretation of the compartments and on whether the transitions correspond to infection events or transmissions among infected states. In this notation, the DFE is $(0, y_0)$. The functions $\mathcal{F}_i, \mathcal{V}_i$ and the disease-free subsystem are supposed to satisfy several mathematical assumptions, namely:

- (A1) $\mathcal{F}_i(0, y) = 0$ and $\mathcal{V}_i(0, y) = 0 \forall y \geq 0$ and $i = 1, \dots, n$. That is, all the new infections arise solely from secondary infections generated by infected individuals.
- (A2) $\mathcal{F}_i(x, y) \geq 0 \forall x, y \geq 0$, $i = 1, \dots, n$, reflecting the fact that the rate of new infections cannot be negative.
- (A3) $\mathcal{V}_i(x, y) \leq 0$ whenever $x_i = 0$, $i = 1, \dots, n$. Since \mathcal{V}_i represents the outflow from compartment i , these conditions ensure that the flow is inward whenever the compartment is empty.
- (A4) $\sum_{i=1}^n \mathcal{V}_i(x, y) \geq 0 \forall x, y \geq 0$, implying that the total outflow from the set of infected compartments is non-negative.
- (A5) The disease-free subsystem $\dot{y} = g(0, y)$ has a unique equilibrium, DFE, which is asymptotically stable.

If system (12) satisfies assumptions (A1)-(A5), the linearization of the disease compartment around the DFE $(0, y_0)$ can be written as

$$\dot{x} = (F - V)x, \quad \text{where} \quad F = \frac{\partial \mathcal{F}_i}{\partial x_j}(0, y_0), \quad V = \frac{\partial \mathcal{V}_i}{\partial x_j}(0, y_0), \quad i = 1, \dots, n, \quad j = 1, \dots, m. \quad (13)$$

It was shown in [25] that the local stability of system $\dot{x} = \mathcal{F}(x, y) - \mathcal{V}(x, y)$ around the DFE $(0, y_0)$ is determined by the linear stability of (13). Furthermore, the matrix FV^{-1} is referred to as the next generation matrix. Defining $\mathcal{R}_0 = \rho(FV^{-1})$, as its spectral radius, the following result holds: the DFE $(0, y_0)$ is locally asymptotically stable if $\mathcal{R}_0 < 1$ and unstable if $\mathcal{R}_0 > 1$.

In our case, the disease compartment satisfies the ODE

$$\begin{pmatrix} \dot{I}_0 \\ \dot{I}_1 \end{pmatrix} = \begin{pmatrix} \beta_{00}SI_0 \\ \beta_{01}SI_0 + \beta_{11}SI_1 \end{pmatrix} - \begin{pmatrix} (\pi_0 + \delta_0)I_0 \\ (\pi_1 + \delta_1)I_1 \end{pmatrix} = \mathcal{F}(X) - \mathcal{V}(X), \quad (14)$$

and the disease-free subsystem is given by

$$\begin{pmatrix} \dot{S} \\ \dot{R} \\ \dot{D} \end{pmatrix} = \begin{pmatrix} -(\beta_{00} + \beta_{01})SI_0 - \beta_{11}SI_1 + \chi R \\ \pi_0 I_0 + \pi_1 I_1 - \chi R \\ \delta_0 I_0 + \delta_1 I_1 \end{pmatrix} = g(X),$$

where $X = (S, I_0, I_1, R, D)$. It is straightforward to check that these two subsystems verify assumptions (A1)-(A4). Regarding (A5) we have:

- (a) DFE point $(S, R, D) = (1, 0, 0)$ is an equilibrium point of $\dot{y} = g(0, y)$.
- (b) To prove that $(1, 0, 0)$ is asymptotically stable it is enough to see that any solution with initial conditions $(S(0), R(0), D(0)), D(0) = 0$ (no deaths) and $S(0) + R(0) = 1$ tends to $(1, 0, 0)$ as t goes to $+\infty$. Indeed, on one hand we have

$$\dot{R} = -\chi R \Rightarrow R(t) = e^{-\chi t}R(0) \Rightarrow \lim_{t \rightarrow +\infty} R(t) = 0,$$

and $\dot{D} = 0$, which implies $D(t) = 0 \ \forall t \geq 0$. On the other, from $\dot{S} = \chi R$ and the expression for $R(t)$ it follows that

$$S(t) = S(0) + \chi \int_0^t R(s) ds = S(0) + \chi R(0) \int_0^t e^{-\chi s} ds = S(0) + R(0) (1 - e^{-\chi t})$$

and so $S(t) \rightarrow 1$ as $t \rightarrow +\infty$, which finally proves (A5).

Thus, the linearization of system (14) around the DFE point leads to

$$\begin{aligned} \begin{pmatrix} \dot{I}_0 \\ \dot{I}_1 \end{pmatrix} &= \left(\begin{pmatrix} \beta_{00}S & 0 \\ \beta_{01}S & \beta_{11}S \end{pmatrix} \Big|_{\text{DFE}} - \begin{pmatrix} \pi_0 + \delta_0 & 0 \\ 0 & \pi_1 + \delta_1 \end{pmatrix} \Big|_{\text{DFE}} \right) \\ &= \begin{pmatrix} \beta_{00} & 0 \\ \beta_{01}\nu_0 & \beta_{11} \end{pmatrix} - \begin{pmatrix} \pi_0 + \delta_0 & 0 \\ 0 & \pi_1 + \delta_1 \end{pmatrix} = F - V. \end{aligned}$$

The NGM is

$$K = FV^{-1} = \begin{pmatrix} \frac{\beta_{00}}{\pi_0 + \delta_0} & 0 \\ \frac{\beta_{01}}{\pi_0 + \delta_0} & \frac{\beta_{11}}{\pi_1 + \delta_1} \end{pmatrix},$$

and, consequently, the basic reproduction number is

$$\mathcal{R}_0 = \rho(FV^{-1}) = \max \left\{ \frac{\beta_{00}}{\pi_0 + \delta_0}, \frac{\beta_{11}}{\pi_1 + \delta_1} \right\},$$

which corresponds to the maximum between the basic reproduction numbers of both viral strains when they are assumed to occur independently. However, recall that in the DFE case, $I_0 = I_1 = 0$, we have defined $\nu_0 = 0$ and $\nu_1 = 0$ and therefore

$$\beta_{01} = \beta_{01}(v_1(0)) = \frac{a_1 \nu_0 v_1(0)}{b_1 + \nu v_1(0)} = 0 \quad \text{and} \quad \beta_{11} = \beta_{11}(v_1(0)) = \frac{a_1 \nu_1 v_1(0)}{b_1 + (1 - \nu)v_1(0)} = 0.$$

Hence, the basic reproduction number is given by

$$\mathcal{R}_0 = \rho(FV^{-1}) = \frac{\beta_{00}}{\pi_0 + \delta_0}, \quad (15)$$

This is natural since, at the very beginning, the unique strain infecting is the master one. The quotient $\beta_{00}/(\pi_0 + \delta_0)$ represents the proportion between the infectious I_0 -inflow (β_{00} , infection) and outflow ($\pi_0 + \delta_0$ immunization and death) rates.

3.3 On the condition for pandemic growth

In analogy with epidemic models based on the instantaneous effective reproduction number - often denoted by \mathcal{R}_t when it varies in time - the goal of this section is to derive a condition that ensures pandemic growth and to relate it to the dynamics of both infected populations. Focusing first on individuals infected by the master strain, we obtain

$$\dot{I}_0 = (\beta_{00}S - (\pi_0 + \delta_0))I_0,$$

which leads to the definition of

$$\mathcal{R}_t^{(0)} = \frac{\beta_{00}}{\pi_0 + \delta_0}S, \quad \text{if } I_0 \neq 0,$$

where $S = S(t)$ and

$$\beta_{00} = \frac{a_0 v_0(t)}{b_0 + v_0(t)}.$$

This is the standard definition for the (time) reproduction number in a one-strain epidemic. It satisfies that I_0 grows if and only if $I_0 \neq 0$ and $\mathcal{R}_t^{(0)} > 1$. We can analogously seek for a condition of I_1 -infected individuals. Thus, for $I_1 \neq 0$, it follows that

$$\dot{I}_1 = (\beta_{01}I_0 + \beta_{11}I_1)S - (\pi_1 + \delta_1)I_1 > 0$$

is equivalent to $\mathcal{R}_t^{(1)} > 1$, for

$$\mathcal{R}_t^{(1)} = \frac{1}{\pi_1 + \delta_1} \left(\beta_{01} \frac{I_0}{I_1} + \beta_{11} \right) S, \quad (16)$$

where $S = S(t)$, $I_j = I_j(t)$, $j = 0, 1$, and

$$\beta_{01} = \frac{a_1 \nu v_1(t)}{b_1 + \nu v_1(t)} \quad \text{and} \quad \beta_{11} = \frac{a_1 (1 - \nu) v_1(t)}{b_1 + (1 - \nu) v_1(t)},$$

where recall that we denote $\nu_0 = \nu$ and $\nu_1 = 1 - \nu$ when $0 < \nu_0 < 1$. Let us now compare the conditions above with the one ensuring the growth of the pandemic whatever the strain (master or mutant) is causing it. This is equivalent to impose that $\dot{I}_0 + \dot{I}_1 > 0$. Indeed,

$$\begin{aligned} \dot{I}_0 + \dot{I}_1 &= \left((\beta_{00} + \beta_{01})I_0 + \beta_{11}I_1 \right) S - (\pi_0 + \delta_0)I_0 - (\pi_1 + \delta_1)I_1 > 0 \\ \Leftrightarrow \mathcal{G}_t &= (\pi_0 + \delta_0)I_0 \left(\mathcal{R}_t^{(0)} - 1 \right) + (\pi_1 + \delta_1)I_1 \left(\mathcal{R}_t^{(1)} - 1 \right) > 0. \end{aligned} \quad (17)$$

Notice that the terms $(\pi_j + \delta_j)I_j$, for $j = 0, 1$, in the expression (17) above correspond to the outflow (either by immunisation or death) of infectious population density I_j . If we denote by

$$\mathcal{O}_t^{(j)} = (\pi_j + \delta_j)I_j(t), \quad j = 0, 1,$$

the outflow rate at time t of I_j , then $\mathcal{G}_t > 0$ is equivalent to

$$\mathcal{G}_t = \mathcal{O}_t^{(0)} \left(\mathcal{R}_t^{(0)} - 1 \right) + \mathcal{O}_t^{(1)} \left(\mathcal{R}_t^{(1)} - 1 \right) > 0. \quad (18)$$

Remark 2 Let us denote by

$$R_t^{(1)} = \frac{\beta_{11}}{\pi_1 + \delta_1} S(t)$$

the corresponding R_t value of a pandemic driven uniquely by the mutant variant (v_1 , and so I_1 only). From (16) and the expression above, it turns out that

$$\mathcal{R}_t^{(1)} = \frac{\beta_{01}}{\pi_1 + \delta_1} \frac{I_0}{I_1} + R_t^{(1)},$$

which relates the R_t values of a v_1 mutant driven pandemic when I_1 acts alone, i.e. $R_t^{(1)}$, and when it comes from a mutation/competition relation with its master virus sequence, i.e. $\mathcal{R}_t^{(1)}$. Notice that

$$\frac{\mathcal{R}_t^{(1)}}{R_t^{(1)}} = 1 + \frac{\beta_{01}}{\beta_{11}} \frac{I_0}{I_1} > 1$$

being, therefore

$$\mathcal{R}_t^{(1)} > R_t^{(1)},$$

both of them computed assuming the same quantity $S(t)$ of susceptible individuals at time t .

3.4 Case of interest 1: a vaccine-like viral strain.

One illustrative scenario chosen to demonstrate the applicability of the model concerns the emergence of a mutant strain that elicits a faster recovery than its master strain, i.e. $\pi_1 > \pi_0$, while both strains are nonlethal ($\delta_0 = \delta_1 = 0$). Several real examples fall within this vaccine-like regime. The best-documented case is Sabine's live attenuated oral poliovirus vaccine type 2 (OPV2), which replicates in the gut, induces strong mucosal immunity, and can secondarily spread to close contacts, thereby boosting herd immunity [28,29]. This example maps directly onto our case assumptions: low δ_1 , high π_1 , and transmission rates tied to fecal viral load, such that larger v_1 drives β_{11} toward saturation. OPV's historic impact stems from this benign circulation, tempered by the rare risk of genetic reversion to circulating vaccine-derived poliovirus (cVDPV) —exactly the mutation-selection tension our framework captures via $\mu_c(\nu)$. From 2021–2025, Novel OPV2 (nOPV2) was deployed at scale to preserve OPV's mucosal and transmission benefits while improving genetic stability. Field and laboratory data show substantially fewer emergences than OPV2, consistent with an avirulent, strongly immunizing agent that can circulate without appreciable mortality, squarely “vaccine-like” [30].

A second example is the live-attenuated rotavirus vaccines. They are shed in stool following the first dose, and although documented transmission to contacts is uncommon, it can confer indirect protection [31]. Recent studies link shedding to seroconversion, and surveillance data report very low transmission without symptomatic disease in exposed infants [32], again matching high π_1 , $\delta_1 \approx 0$, and a typically low-to-moderate, short-lived $\beta_{11}(v_1)$ as the recovered population accumulates.

The assumptions $\pi_1 > \pi_0$ and $\delta_0 = \delta_1 = 0$ allow, in principle (Section 3.1), the existence of all four types of steady states: DFE, NME, NmutE, and CSE equilibria. Another direct implication of $\delta_0 = \delta_1 = 0$ is that $\dot{D} = \delta_0 I_0 + \delta_1 I_1 = 0$ and so D is a first integral. Recall that the total mass $S + I_0 + I_1 + R + D$ is also a first integral of the macroscopic system. Since it is expected that, at the beginning of the process, $D(0) = 0$, henceforth it will be assumed that $D(t) = 0 \forall t \geq 0$ and D will be excluded from further analysis.

For a first numerical exploration, we have conveniently fixed the following parameters

$$\begin{aligned} \chi &= 2, & \pi_0 &= 0.5, & f_0 &= 1, & \xi_0 &= 2, & \gamma_0 &= 0.8, \\ a_0 &= 4, & b_0 &= 0.1, & \xi_1 &= 1, & \gamma_1 &= 0.5, & b_1 &= 0.1, \end{aligned} \tag{19}$$

with $\delta_0 = \delta_1 = 0$ and the ratio between the slow and fast time scales equal to $\varepsilon = 0.01$. For values of the recovery rate $\pi_1 > \pi_0$, the mutant fitness f_1 , the maximal potential threshold for β_{01} and β_{11} , and the master's mutation error μ , ranging in suitable intervals, we compute the ω -limit of the trajectory starting with initial conditions

$$(S, I_0, I_1, R, D) \times (g_0, g_1; v_0, v_1) = (1 - 10^{-4}, 10^{-4}, 0, 0, 0) \times (1, 0; 0, 0). \tag{20}$$

Along the paper, we will refer to the solution with these i.c. as the principal trajectory. According to the type of equilibrium point reached (its ω -limit), for any choice of the latter parameters, we paint (Figure 3A) the corresponding point in the parameter's space with colors: **NME**, **DFE**, and **CSE**. In Figure 3B the time evolution of the macroscopic and microscopic variables, respectively, for three particular choices of these parameters is shown. To analyze the variation of the ω -limit (and its time evolution) of this principal trajectory in terms of the mutant recovery π_1 , we fix the rest of parameters as $a_1 = 6$, $f_1 = 0.2$, and $\mu = 0.675$.

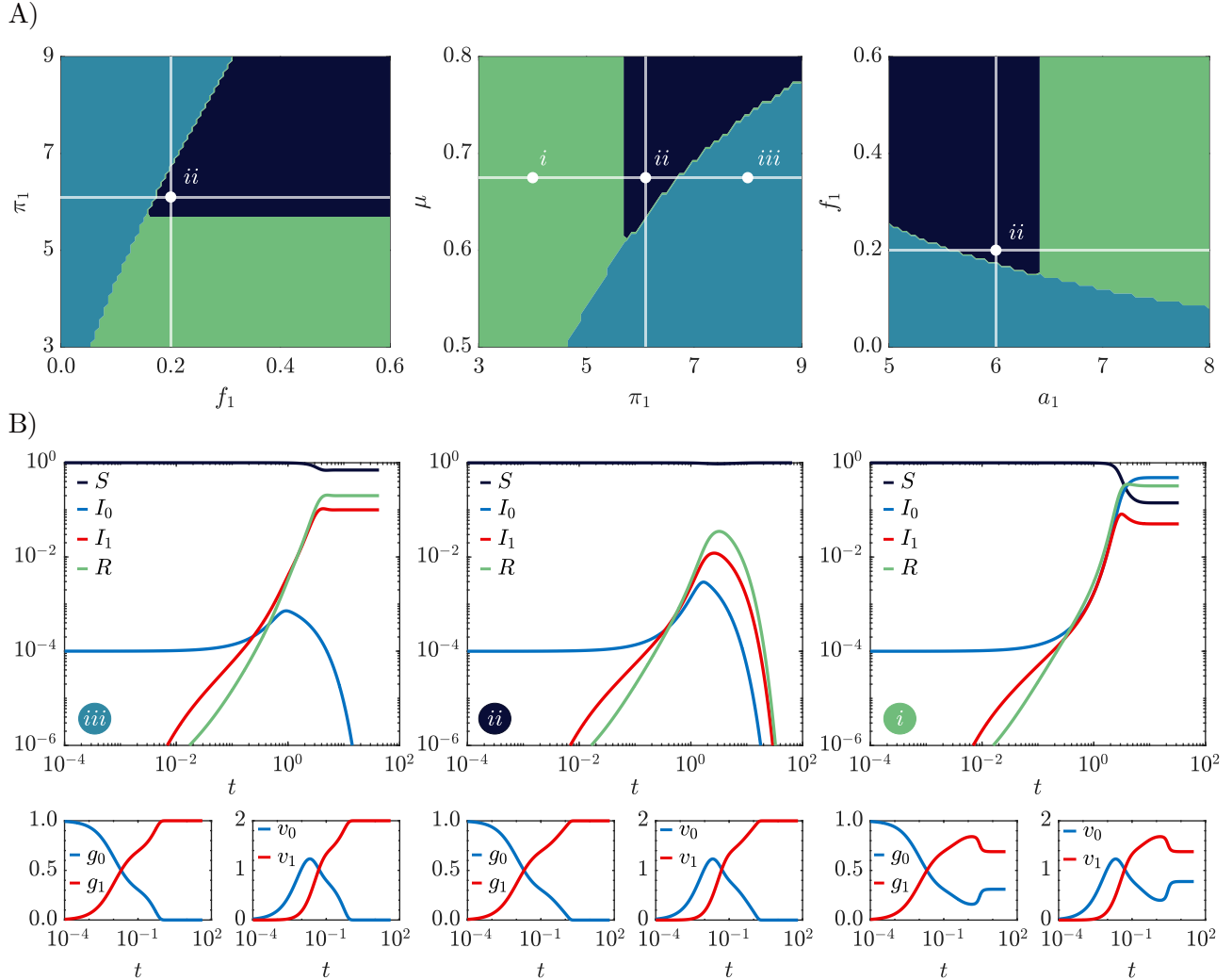


Figure 3: (A) ω -limits of the principal trajectory with i.c. (20) and fixed parameters (19) for three different combinations of parameters. Each point of the plot is colored according to the type of equilibrium reached: **NME**, **DFE**, and **CSE**. The first and second panels correspond to $a_1 = 6$, while the third one fixes $\mu = 0.675$. These, together with $f_1 = 0.2$, will be the nominal values employed for the case study. They are highlighted in the plots using solid white lines to facilitate visual reference. (B) Time evolution of the macroscopic and microscopic variables for three scenarios, highlighted in the upper panel. Each simulation illustrates convergence toward a different equilibrium.

Figure 3 suggests the following points to investigate in terms of π_1 : (a) the existence of equilibrium points and their types; (b) their local stability and multistability scenarios and, when possible, (c) to find out mechanisms underlying changes in the ω -limit of the principal trajectory with i.c. (20).

3.4.1 Equilibrium points

The existence and expression of these equilibria follow from the propositions in Section 3.1. Further analysis will show how variations in the host immune response (encoded in the value of π_1) influence their behavior. We will particularly be concerned with the possibility of co-circulation of both the master and the mutant viral strains. Recall that $D \equiv 0$ will be always assumed. Thus, regarding the equilibrium points in this particular case, it follows that:

- **Disease-free equilibrium (DFE)**

They are of the form

$$\text{DFE : } (S^*, I_0^*, I_1^*, R^*, D^*) \times (g_0^*, g_1^*, v_0^*, v_1^*) = (1, 0, 0, 0, 0) \times \left(g_0^*, 1 - g_0^*, \frac{\xi_0}{\gamma_0} g_0^*, \frac{\xi_1}{\gamma_1} (1 - g_0^*) \right),$$

for $g_0^* \in [0, 1]$. However, they represent a segment in the full system space, and so there are infinitely many of them, in terms of the macroscopic equilibrium they correspond to the same steady state $(S^*, I_0^*, I_1^*, R^*, D^*) = (1, 0, 0, 0)$.

- **No master equilibrium (NME).**

From Proposition 2, the only microscopic equilibrium is given by $(g_0, g_1) = (0, 1)$ which, in its turn, yields to

$$(v_0, v_1) = \left(0, \frac{\xi_1}{\gamma_1} \right) \quad \text{and} \quad \beta_{00} = 0, \quad \beta_{01} = 0, \quad \beta_{11} = \frac{a_1 \frac{\xi_1}{\gamma_1}}{b_1 + \frac{\xi_1}{\gamma_1}}.$$

From the expression for the I_1 equilibrium, the following constraint is derived:

$$I_1^* = \frac{1 - \frac{\pi_1}{\beta_{11}}}{1 + \frac{\pi_1}{\chi}} \in (0, 1) \Rightarrow 1 - \frac{\pi_1}{\beta_{11}} > 0 \Rightarrow \pi_1 < \beta_{11} \Leftrightarrow \pi_1 < \frac{a_1 \xi_1}{b_1 \gamma_1 + \xi_1},$$

which in our particular case reads $\pi_1 < 40/7$. If such condition holds, the expression for the unique NME equilibrium is

$$\text{NME : } (S^*, I_0^*, I_1^*, R^*, D^*) \times (g_0^*, g_1^*, v_0^*, v_1^*) = \left(\frac{\pi_1}{\beta_{11}}, 0, \frac{1 - \frac{\pi_1}{\beta_{11}}}{1 + \frac{\pi_1}{\chi}}, \frac{\pi_1}{\chi} \cdot \frac{1 - \frac{\pi_1}{\beta_{11}}}{1 + \frac{\pi_1}{\chi}}, 0 \right) \times \left(0, 1; 0, \frac{\xi_1}{\gamma_1} \right).$$

- **No mutant equilibrium (NmutE)**

There are no equilibrium points of this type. Briefly, the only possible microscopic solutions $(g_0, g_1) = (1 - \mu, \mu)$ with $0 \leq \mu < 1$ lead to

$$(v_0, v_1) = \left(\frac{\xi_0}{\gamma_0} (1 - \mu), \frac{\xi_1}{\gamma_1} \mu \right) \quad \text{and} \quad \beta_{00} = \frac{a_0 \frac{\xi_0}{\gamma_0} (1 - \mu)}{b_0 + \frac{\xi_0}{\gamma_0} (1 - \mu)}, \quad \beta_{01} = \frac{a_1 \frac{\xi_1}{\gamma_1} \mu}{b_1 + \frac{\xi_1}{\gamma_1} \mu}, \quad \beta_{11} = 0.$$

From the third equation of the macroscopic system, $\beta_{01} I_0 S = 0$, it turns out that either $S = 0$ or $\beta_{01} = 0$ (i.e., $a_1 = 0$). The first of both cases, $S = 0$, does not lead to any equilibrium solution since it leads to $\pi_0 I_0 = 0$, which is not possible. On the other hand, from the third equation of the macroscopic system, $\beta_{01} I_0 S = 0$, it follows that either $S = 0$ or $\beta_{01} = 0$. The first case, $S = 0$ implies again that $\pi_0 I_0 = 0$, a contradiction. The second case is only possible if $a_1 = 0$ (a non-transmissible mutant), which is not the case under consideration.

- **Co-circulating strains equilibrium (CSE)**

This is the most general and intricated case, as it is subject to the fewest restrictions. We seek for equilibrium points with both infected populations nonvanishing. This implies that $\nu^* = \nu(I_0^*, I_1^*) \in (0, 1)$ and, according to the Swetina-Schuster model, the genomes' equilibrium are given either by

$$(g_0^*, g_1^*) = \left(1 - \frac{\mu}{\mu_c^*}, \frac{\mu}{\mu_c^*} \right) \quad \text{if } 0 < \mu < \mu_c^*,$$

or $(g_0, g_1) = (0, 1)$ (master genome's extinction) if $\mu_c^* \leq \mu \leq 1$, where we recall that

$$\mu_c^* = 1 - \frac{f_1}{f_0} \left(\frac{1}{\nu^*} - 1 \right)$$

Let us analyze both cases separately.

(i) Case $0 < \mu < \mu_c^*$.

Here we have:

$$(g_0^*, g_1^*) = \left(1 - \frac{\mu}{\mu_c^*}, \frac{\mu}{\mu_c^*} \right), \quad (v_0^*, v_1^*) = \left(\frac{\xi_0}{\gamma_0} g_0^*, \frac{\xi_1}{\gamma_1} g_1^* \right),$$

and

$$\beta_{00}^* = \frac{a_0 v_0^*}{b_0 + v_0^*}, \quad \beta_{01}^* = \frac{a_1 \nu^* v_1^*}{b_1 + \nu^* v_1^*}, \quad \beta_{11}^* = \frac{a_1 (1 - \nu^*) v_1^*}{b_1 + (1 - \nu^*) v_1^*},$$

Notice that β_{00}^* , β_{01}^* , and β_{11}^* are all three strictly positive. On the other side, from Proposition 4 the following expressions for the macroscopic variables at equilibrium hold:

$$S^* = \frac{\pi_0}{\beta_{00}^*} \quad R^* = \frac{\pi_0 I_0^* + \pi_1 I_1^*}{\chi}, \quad I_1^* = I_0^* \left(\frac{\beta_{01}^* \pi_0}{\beta_{00}^* \pi_1 - \beta_{11}^* \pi_0} \right). \quad (21)$$

Hence, a necessary condition for the existence of I_1^* (and, therefore, of CSE) is that

$$\frac{\pi_0}{\beta_{00}^*} < \frac{\pi_1}{\beta_{11}^*}.$$

If it holds, macroscopic CSE solutions must satisfy

$$S^* + I_0^* + I_1^* + R^* = 1 \Leftrightarrow \frac{\pi_0}{\beta_{00}^*} + I_0^* + I_0^* \left(\frac{\beta_{01}^* \pi_0}{\beta_{00}^* \pi_1 - \beta_{11}^* \pi_0} \right) + \frac{\pi_0 I_0^* + \pi_1 I_1^*}{\chi} = 1$$

or, equivalently, $\mathcal{F}(I_0^*, I_1^*) = 0$, where

$$\mathcal{F}(I_0^*, I_1^*) = \frac{\pi_0}{\beta_{00}^*} + I_0^* + I_0^* \left(\frac{\beta_{01}^* \pi_0}{\beta_{00}^* \pi_1 - \beta_{11}^* \pi_0} \right) + \frac{\pi_0 I_0^* + \pi_1 I_1^*}{\chi} - 1.$$

This is an involved (but rational) equation in I_0^* , I_1^* since β_{01}^* , and β_{11}^* , in turn, also depend on them through ν^* . This equation has been numerically solved in Figure 4).

Remark 3 At this CSE equilibrium, the I_0 and I_1 -reproduction numbers (see Section 3.3) at the equilibrium,

$$\mathcal{R}_*^{(0)} = \frac{\beta_{00}^*}{\pi_0} S^*, \quad \mathcal{R}_*^{(1)} = \frac{1}{\pi_1} \left(\beta_{01}^* \frac{I_0^*}{I_1^*} + \beta_{11}^* \right) S^*,$$

are both equal to 1. Indeed, first, having in mind (21), it follows that

$$\mathcal{R}_*^{(0)} = \frac{\beta_{00}^*}{\pi_0} S^* = \frac{\beta_{00}^*}{\pi_0} \frac{\pi_0}{\beta_{00}^*} = 1.$$

Regarding the second assertion:

$$\mathcal{R}_*^{(1)} = \frac{\pi_0}{\beta_{00}^* \pi_1} \left(\beta_{01}^* \cdot \frac{\beta_{00}^* \pi_1 - \beta_{11}^* \pi_0}{\beta_{01}^* \pi_0} + \beta_{11}^* \right) = \frac{1}{\beta_{00}^* \pi_1} (\beta_{00}^* \pi_1 - \beta_{11}^* \pi_0 + \beta_{11}^* \pi_0) = 1.$$

(ii) Case $\mu_c \leq \mu \leq 1$.

In this scenario, there are no equilibrium points of this type. Indeed, the microscopic equilibrium is $(g_0, g_1, v_0, v_1) = (0, 1, 0, \xi_1/\gamma_1)$, which means $\beta_{00} = 1$. But this implies $\dot{I}_0 = -\pi_0 I_0 = 0$ which can be only satisfied if $\pi_0 = 0$ or $I_0 = 0$, in contradiction with our assumptions.

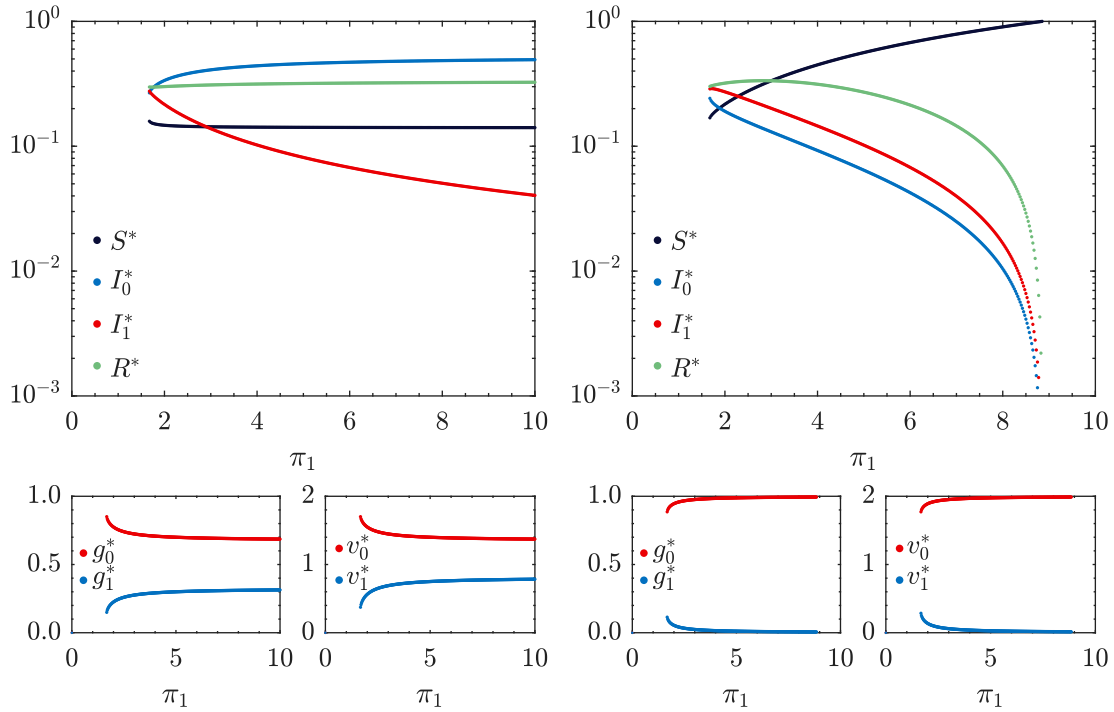


Figure 4: Co-circulating strains equilibrium points, computed numerically, as a function of $\pi_1 \in (\pi_0, 10) = (0.5, 10)$. If we define $\pi_1^\dagger \simeq 1.675$ and $\pi_1^\diamond \simeq 8.875$ then: for $\pi_1 \in (\pi_0, \pi_1^\dagger)$ there is no equilibrium point; for $\pi_1 \in (\pi_1^\dagger, \pi_1^\diamond)$ there are two, and for $\pi_1 \in (\pi_1^\diamond, 10)$ there is only one. They are plotted in the left and right panels above (top: macroscopic, bottom: microscopic). These two families of CSE equilibria show relevant differences: on one side, family CSE₁ (left) starts at a point with equal infective individuals $I_0^* = I_1^*$ and exhibits a monotonous decrease of the I_1^* -population as π_1 grows; on the other side, family CES₂ (right) begins with $I_1^* > I_0^*$ and undergoes a bifurcation (namely, collision with the DFE equilibrium $(1, 0, 0, 0)$) as $\pi_1 \rightarrow \pi_1^\diamond$ (see Figure 5).

3.4.2 Equilibria stability

In the previous section, we identified the admissible equilibrium states of the system under the parameter regime of interest. In this section, we analyze the local stability of each equilibrium point by evaluating the corresponding jacobian matrices. Recall that the parameter choices are specified in (19), with $\delta_0 = \delta_1 = 0$, $\varepsilon = 0.01$, and π_1 varying in the interval $(\pi_0, 10)$.

The Jacobian matrix determines the linearized dynamics of the system in the vicinity of an equilibrium, and its eigenvalues determine the local behavior. In particular, an equilibrium is locally asymptotically stable if and only if all eigenvalues of the jacobian have negative real parts. Conversely, the presence of any eigenvalue with a positive real part implies instability. This analysis allow us to identify parameter regions in which qualitative changes in stability occur, providing insights into potential bifurcations and transitions between different dynamical regimes.

- **Disease-free equilibria (DFE).** They are of the form

$$\text{DFE} : (S^*, I_0^*, I_1^*, R^*, D^*) \times (g_0^*, g_1^*, v_0^*, v_1^*) = (1, 0, 0, 0, 0) \times \left(g_0^*, 1 - g_0^*, \frac{\xi_0}{\gamma_0} g_0^*, \frac{\xi_1}{\gamma_1} (1 - g_0^*) \right),$$

parametrized in terms of $g_0^* \in [0, 1]$. Their jacobian have the following spectrum:

$$\lambda_{\text{DFE}} = \left\{ -2, -\frac{4}{5}, -\frac{1}{2}, 0, 0, 0, \frac{175g_0^* - 1}{50g_0^* + 2}, -\pi_1 \right\}.$$

All the eigenvalues are real. Three of them are 0 (associated to the freedom in $I_0 = I_1 = D = 0$), four negative

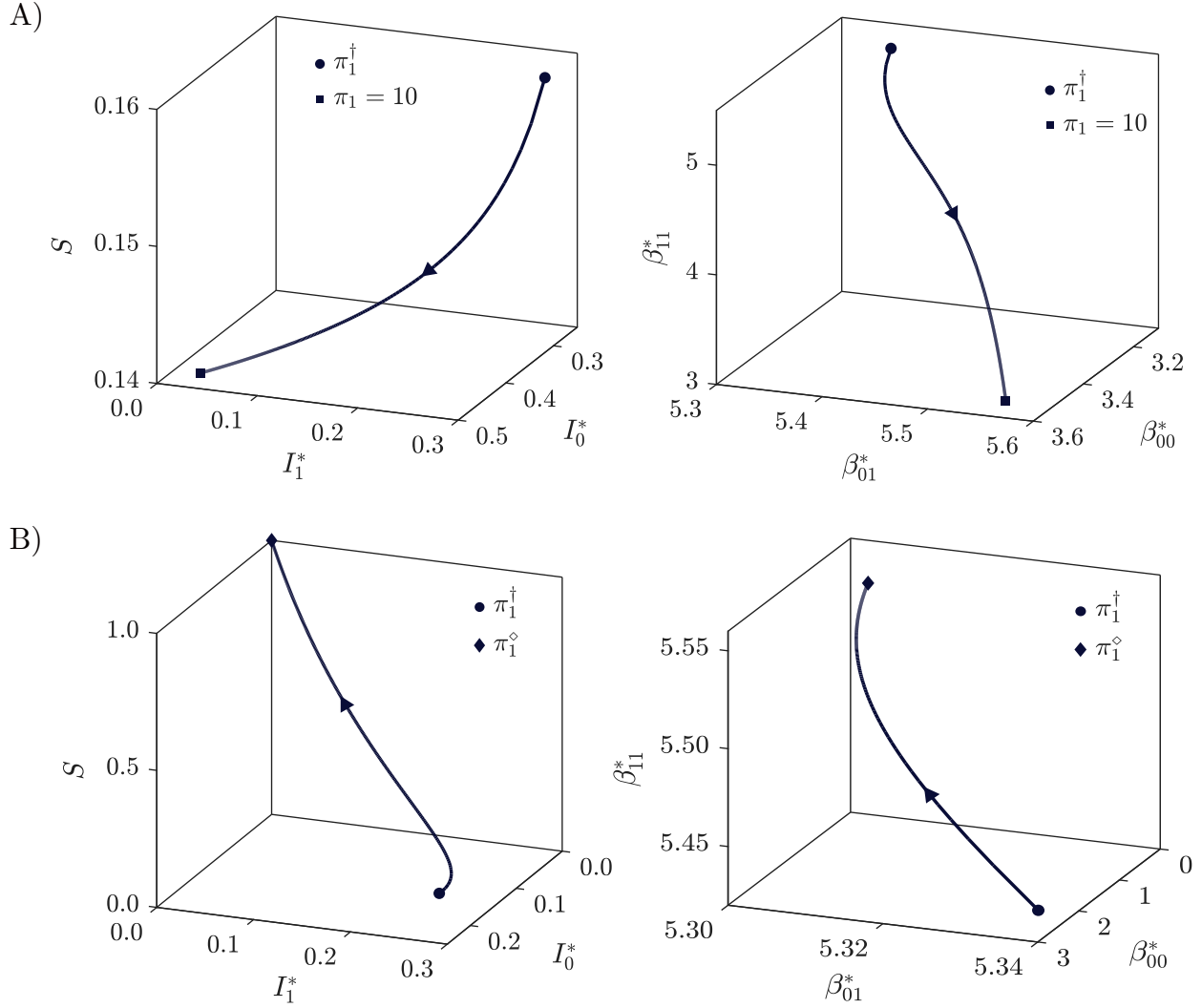


Figure 5: (A) Evolution of the family of CSE₁ points, varying with π_1 (see Figure 4 (left)), for the (S, I_0, I_1) variables (left) and $\beta_{00}^*, \beta_{01}^*$ (right). (B) Mechanism leading the CSE₂ point (see Figure 4(right)) towards its collision with the DSE point $(1, 0, 0, 0)$ as π_1 tends to π_1^\diamond . Left: (S, I_0^*, I_1^*) variables. Right: transmission rates β_{00}^* and β_{01}^* .

and a unique eigenvalue

$$\lambda_{\text{dfe}}(g_0^*) = \frac{175g_0^* - 1}{50g_0^* + 2},$$

exclusively depending on g_0^* , which determines their stability. This was expected since the macroscopic equilibrium is always $(S^*, I_0^*, I_1^*, R^*, D^*) = (1, 0, 0, 0, 0)$. The variation in the complete system equilibrium comes from the microscopic equilibria, given by a segment - parametrized by g_0^* - in the genomes-virions space. Namely, it is easy to check that an DFE is asymptotically stable (indeed, attractor in the normal bundle space to the invariant manifold $\{I_0 = I_1 = D = 0\}$) provided that $g_0^* \in [0, 1/175]$ and unstable (a saddle point) if $g_0^* \in (1/175, 1]$.

Notice that the stability condition is equivalent (as expected) to the basic reproduction number $\mathcal{R}_0 < 1$ defined in (15). Indeed, from the fact that $\beta_{11}^* = 0$, from the values of the parameters in (19), and taking into account that $v_0^* = \xi_0 g_0^* / \gamma_0$, it follows that

$$\mathcal{R}_0 = \frac{\beta_{00}^*}{\pi_0} = \frac{20g_0^*}{0.1 + 2.5g_0^*} < 1 \Leftrightarrow g_0^* < \frac{1}{175},$$

for any value of π_1 .

- **No master equilibrium (NME)**

The spectrum of the jacobian matrix evaluated on the NME points

$$\text{NME : } (S^*, I_0^*, I_1^*, R^*, D^*) \times (g_0^*, g_1^*; v_0^*, v_1^*) = \left(\frac{\pi_1}{\beta_{11}}, 0, \frac{1 - \frac{\pi_1}{\beta_{11}}}{1 + \frac{\pi_1}{\chi}}, \frac{\pi_1}{\chi} \cdot \frac{1 - \frac{\pi_1}{\beta_{11}}}{1 + \frac{\pi_1}{\chi}}, 0 \right) \times \left(0, 1; 0, \frac{\xi_1}{\gamma_1} \right),$$

defined for $\pi_1 < 40/7$, is denoted by

$$\lambda_{\text{NME}} = \left\{ -\frac{4}{5}, -\frac{1}{2}, -\frac{1}{2}, -\frac{1}{5}, -\frac{1}{5}, 0, -\frac{54 - \sqrt{2}\psi}{7(\pi_1 + 2)}, -\frac{54 + \sqrt{2}\psi}{7(\pi_1 + 2)} \right\}$$

with $\psi = \sqrt{\Delta}$ and $\Delta = \Delta(\pi_1) := 49\pi_1^3 - 84\pi_1^2 - 924\pi_1 + 338$. As in the previous case, it has one zero eigenvalue (associated with the neutral (or central) manifold $I_0 = 0$), five real negative eigenvalues, and a couple of complex conjugate eigenvalues

$$\lambda_{\text{nme}^-} = -\frac{54 - \sqrt{2}\psi}{7(\pi_1 + 2)}, \quad \lambda_{\text{nme}^+} = -\frac{54 + \sqrt{2}\psi}{7(\pi_1 + 2)},$$

which can be real or complex depending on the sign of Δ . This discriminant is $\Delta < 0$ if $\pi_1 \in (0.356.., 40/7)$ and $\Delta > 0$ if $\pi_1 < 0.356..$ or $\pi_1 > 40/7$. Figure 6 shows the real and imaginary part of these two eigenvalues as functions of π_1 .

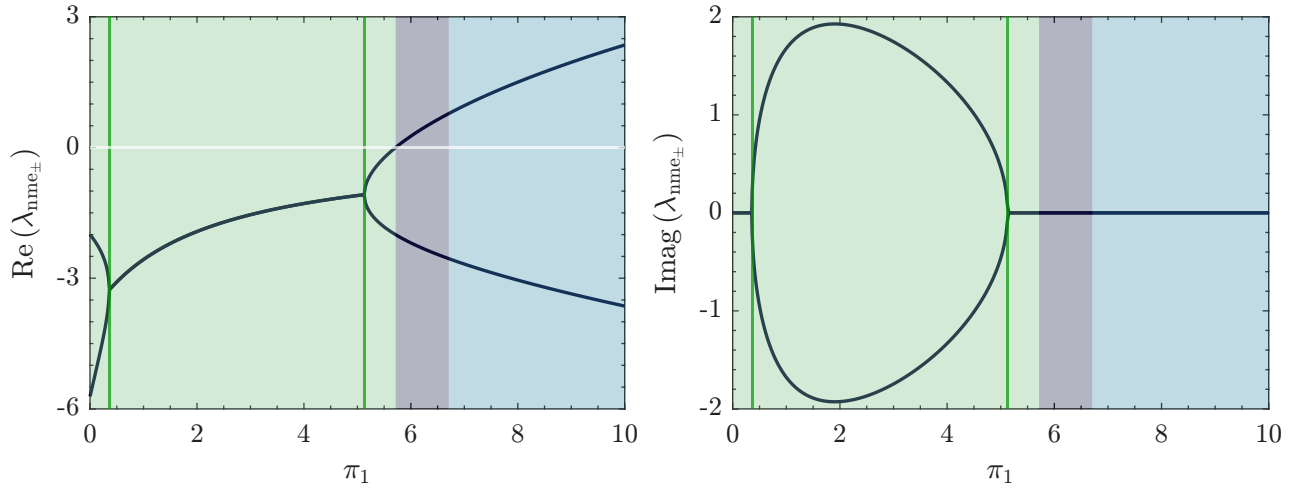


Figure 6: Eigenspectrum of the Jacobian matrix at the NME point. The background color stands for the corresponding numerical ω -limit of the principal trajectory (20), see Figure 3, which are **NME**, **DFE** and **CSE**. The two vertical green lines indicate the region in which the system exhibits complex eigenvalues, *i.e.*, where the Jacobian has eigenvalues with non-zero imaginary parts, corresponding to the interval $\pi_1 \in (0.357.., 5.129..)$.

Therefore, for $\pi_1 \in (\pi_0, 40/7)$, we have two regions of stability according to its value:

(a) Case $\pi_1 \in (\pi_0, 5.128..)$: in this scenario, $\psi = \sqrt{\Delta}$ is complex and so λ_{nme^\pm} are a couple of complex conjugate eigenvalues, namely:

$$\lambda_{\text{nme}^-} = -\frac{54}{7(\pi_1 + 2)} + i \frac{\sqrt{-2\Delta}}{7(\pi_1 + 2)}, \quad \lambda_{\text{nme}^+} = \overline{\lambda_{\text{nme}^-}}$$

Since their real part is negative, the corresponding NME point is attractor (out of the neutral manifold). In the 2-dimensional manifold associated to λ_{nme^\pm} , the trajectories exhibit damped oscillations. It is known that, on this plane, and close to the equilibrium point, the quasi-period of such oscillations is

$$T(\pi_1) \simeq \frac{2\pi}{\text{Im}(\lambda_{\text{nme}^-})} = \frac{\sqrt{2}\pi(7\pi_1 + 2)}{\sqrt{-\Delta}}, \quad (22)$$

where $\Delta = \Delta(\pi_1)$ (Figure 7).

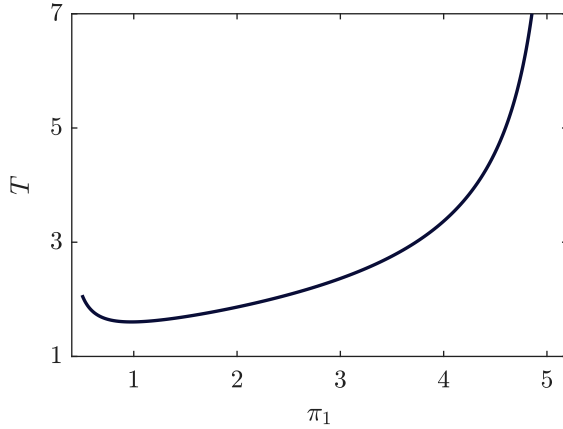


Figure 7: Quasi-period $T(\pi_1)$, see (22), of the damped oscillations in a neighbourhood of the NME point for $\pi_1 \in (1/2, 5.128..)$.

(b) Case $\pi_1(5.128.., 40/7)$: now the discriminant $\Delta > 0$ implies that both $\lambda_{\text{nme}\pm}$ are real. Furthermore, $\lambda_{\text{nme}+} < 0$ and $\lambda_{\text{nme}-} < 0$. Hence, the NME point is stable.

• Co-circulating strains equilibrium (CSE)

For the set of parameters (19) our model has two distinct families of CSE points, denoted as CSE_1 and CSE_2 and found numerically and illustrated in Figure 4. To assess their local stability, we numerically compute their jacobian matrices and calculate their spectrum. Figure 8 shows the results of this analysis.

Figure 8A shows the real and imaginary parts of the eigenvalues as functions of π_1 for the equilibrium point CSE_1 (left panel in Figure 4), for a range of values of the parameter π_1 . In this case, all eigenvalues exhibit negative real parts across this interval, meaning that the equilibrium is asymptotically stable. Nonetheless, the presence of complex conjugate eigenvalues introduces damped oscillatory modes into the local dynamics near the equilibrium. Two eigenvalues, highlighted in orange and yellow, remain a complex conjugate pair across the entire range of π_1 explored. This persistent non-zero imaginary part indicates the existence of an oscillatory mode whose frequency and decay rate vary with π_1 . In contrast, three other eigenvalues (blue, green, and red) alternate between being real and forming complex conjugate pairs. These transitions correspond to bifurcations occurring at critical values of π_1 , denoted π_1^a , π_1^b , π_1^c , and π_1^d in the figure. At these bifurcation points, the corresponding eigenvalues collide on the real axis and subsequently branch off into the complex plane (or *vice versa*), thereby introducing or annihilating additional oscillatory modes. Figure 8B provides a schematic representation of these bifurcations in the complex plane. The trajectories of the blue, green, and red eigenvalues are illustrated to emphasize their transitions between real and complex configurations. Collectively, these bifurcations enrich the system's dynamical landscape, enabling multiple qualitatively distinct oscillatory regimes depending on the parameter π_1 .

Finally, Figure 8C shows the eigenvalue spectrum corresponding to CSE_2 (see the right panel in Figure 4). Across the range of π_1 studied, one eigenvalue exhibits a strictly positive real part, which reveals the instability of CSE_2 . Additionally, two eigenvalues form complex conjugate pairs, indicating the presence of an oscillatory mode, although the dynamics would be ultimately dominated by the unstable direction. This complex conjugate pair also exhibits a bifurcation right before CSE_2 vanishing. Due to the repelling nature of CSE_2 , the simulated principal trajectories will never converge to this equilibrium.

3.4.3 The limit case $\pi_1 \rightarrow +\infty$

An extreme scenario arises when the mutant strain induces a very rapid recovery in the host, $\pi_1 \gg 1$. This regime can be mathematically approximated by taking the limit $\pi_1 \rightarrow +\infty$. In this extreme case, the dynamics resemble a situation in which the master variant gives rise to a mutant strain that lacks self-replicative capacity (see Figure 9). In this setting, the mutant can only increase in frequency due to erroneous replication of the

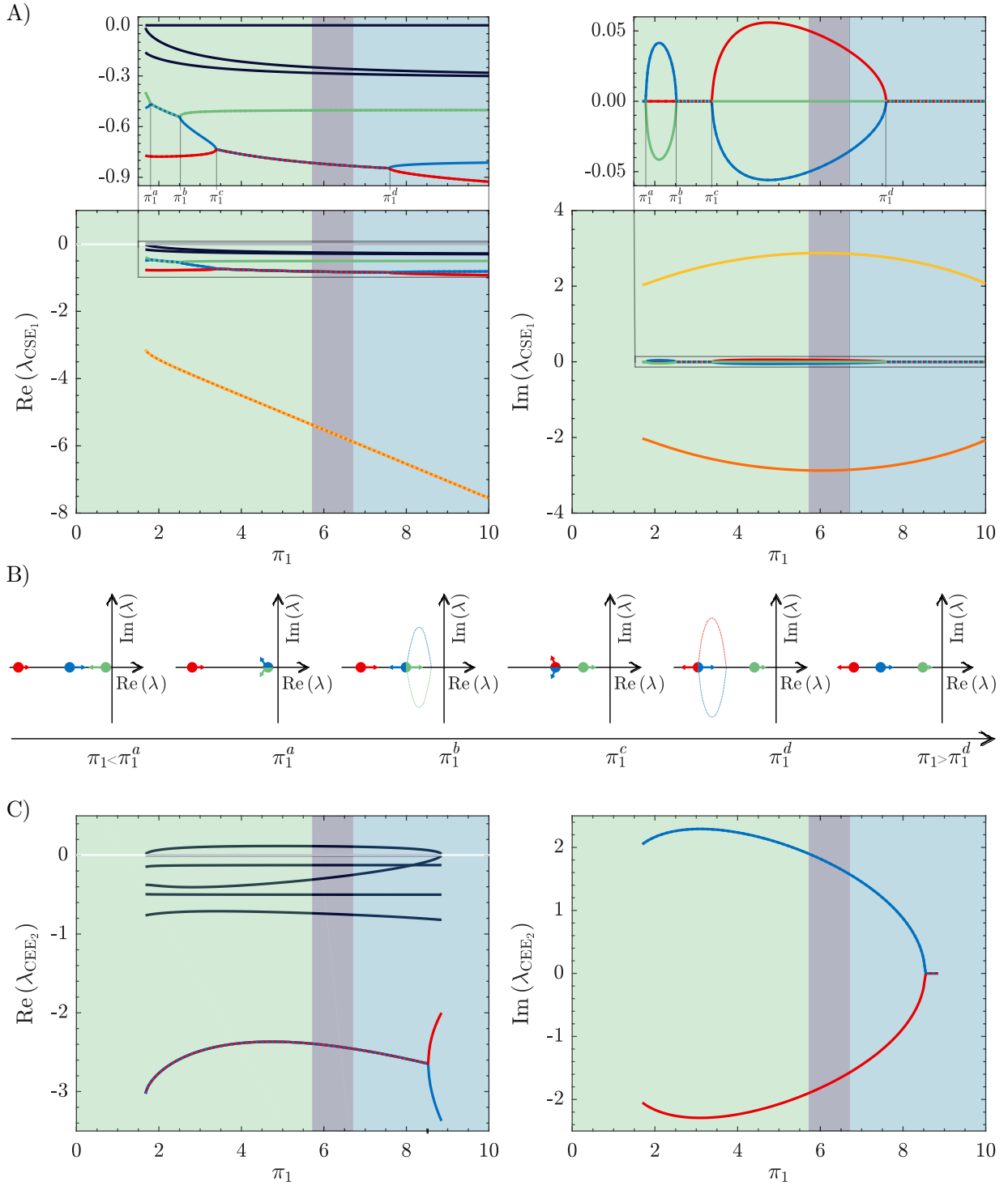


Figure 8: (A) Real (left) and imaginary (right) parts of the eigenvalues associated with the numerically computed equilibrium point CEE_1 . Insets enhance resolution within the grey-marked region. (B) Schematic representation of the evolution of the three eigenvalues undergoing bifurcations at $\pi_1 = \pi_1^j$, with $j = a, b, c, d$ (see main text). (C) Same as (A), for the equilibrium CEE_2 . In (A) and (C), background color indicates the ω -limit of the principal trajectory (Figure 3): **NME**, **DFE**, or **CEE**. Color coding links real and imaginary parts of each eigenvalue; black indicates a vanishing imaginary part.

master genome (g_0), which occasionally produces virions (v_1) capable of infecting new hosts. However, upon infection by this defective strain, the host rapidly recovers and temporarily acquires immunity, governed by the parameter χ .

Under these conditions, we may assume that $I_1 \rightarrow 0$, since recovery is effectively instantaneous. This implies $v_1 \rightarrow 0$ and either $\nu_0 \rightarrow 1$ (when $I_0 \neq 0$) or $\nu_0 \rightarrow 0$ (if $I_0 = 0$). Consequently, $\beta_{11} \rightarrow 0$, $\tilde{f}_1 = f_1 \nu_1 \rightarrow 0$ and either $\tilde{f}_0 = f_0 \nu_0 \rightarrow f_0$ (if $I_0 \neq 0$) or $\tilde{f}_0 = f_0 \nu_0 \rightarrow 0$ (if $I_0 = 0$). Henceforth, we assume that all variables and parameters take their corresponding limiting values.

From Section 3.4.2, we know that two type of equilibrium points exist in this limit: the DFE and the CSE. In the former case, $I_0 = 0$ implies $\nu_0 = 0$ and $\tilde{f}_0 = 0$, leading to a trivial genomic system $\dot{g}_0 = 0$, $\dot{g}_1 = 0$. Its equilibrium solutions are of the form $(g_0^*, 1 - g_0^*)$ for $g_0^* \in [0, 1]$. Together with the corresponding virion equilibria, these states yield to the previously defined QS_{mic} (see Proposition 1). In this case, it is straightforward to show that the unique macroscopic DFE is $(S^*, I_0^*, R^*) = (1, 0, 0)$. In contrast, in the CSE case, when $I_0 > 0$, the microscopic system becomes

$$\dot{g}_0 = f_0 g_0 (1 - \mu - g_0), \quad \dot{g}_1 = f_0 g_0 (\mu - g_0),$$

for $0 < \mu < 1$. This system has two equilibrium points: $(g_0^*, g_1^*) = (0, 1)$ (repeller) and $(g_0^*, g_1^*) = (1 - \mu, \mu)$ (attractor), which derive into

$$(v_0^*, v_1^*) = \left(0, \frac{\xi_1}{\gamma_1} \right) \quad \text{and} \quad (v_0^*, v_1^*) = \left(\frac{\xi_0}{\gamma_0} (1 - \mu), \frac{\xi_1}{\gamma_1} \mu \right),$$

respectively, for the virion equilibria. In this scenario, the macroscopic system reads

$$\dot{S} = -(\beta_{00} + \beta_{01}) I_0 S + \chi R, \quad \dot{I}_0 = (\beta_{00} S - \pi_0) I_0, \quad \dot{R} = \beta_{01} I_0 S + \pi_0 I_0 - \chi R.$$

Notice that $v_0^* = 0$ implies $\beta_{00} = 0$ and so, from the second equation above, that $\pi_0 = 0$ (since $I_0 > 0$), a contradiction with the fact that we are assuming $\pi_0 = 2$ in this section. The second microscopic equilibrium solution is $\text{QS}_{\text{mic}}^{(\mu)}$,

$$(g_0^*, g_1^*; v_0^*, v_1^*) = \left(1 - \mu, \mu; \frac{\xi_0}{\gamma_0} (1 - \mu), \frac{\xi_1}{\gamma_1} \mu \right)$$

already defined in (A1). The corresponding equilibrium for the macroscopic system is easily derived:

$$S^* = \frac{\pi_0}{\beta_{00}}, \quad I_0^* = \frac{\chi}{\chi + \left(1 + \frac{\beta_{01}}{\beta_{00}} \right) \pi_0}, \quad R^* = 1 - S^* - I_0^*, \quad (23)$$

such that the three variables sum 1.

Concerning their local stability, the computation of the spectra of their associated jacobian matrices, gives rise to: (a) $\{-\chi_1, \beta_{00} - \pi_0\}$ for the DFE point $(1, 0, 0)$, which means that it is stable if $\pi_0 > \beta_{00}$ (*i.e.*, it has $\mathcal{R}_0 < 1$) and unstable otherwise; (b) for the CSE point (23), it is straightforward to show that its determinant is positive, the trace negative and, hence, it is always stable. Furthermore, its behavior moves between a stable node or focus (so, oscillations appear) depending on the values of β_{00} , β_{01} , π_0 , and χ . These parameters also determine, in the cases of bistability, the configuration of the corresponding basins of attraction.

Biologically, this setting is reminiscent of defective viral genomes (DVGs) which, despite their inability to autonomously sustain a replication cycle by themselves, can still be packaged into master-encoded viral particles and transmitted [33]. Although such transmission does not establish a productive infection, it may nevertheless be sufficient to trigger an immune response in the host, for example through superinfection exclusion or the induction of immune memory. Indeed, this property has opened the tantalizing possibility of using engineered versions of DVGs as self-transmissible vaccines [34].

3.5 Case of interest 2: the burnout viral strain.

Below, we highlight three well-documented examples that lie near the burnout corner of our parameter space, characterized by very high virulence ($\delta_1 \gg 0$), transmission rate sufficient to ignite large outbreaks (effectively

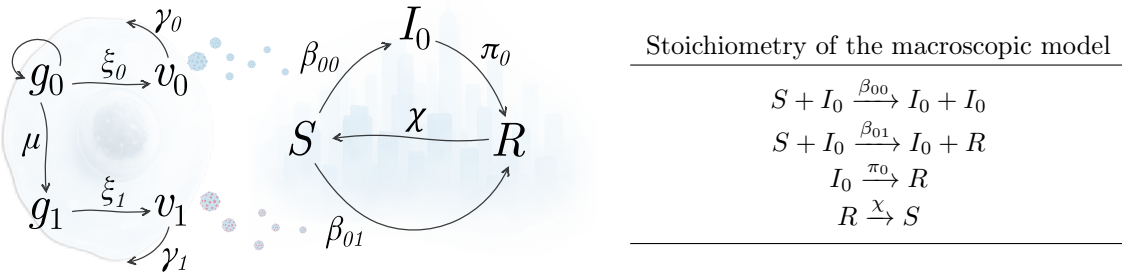


Figure 9: (left) Schematic representation of the reduced model in the limit case $\pi_1 \rightarrow \infty$. (Right) Macroscopic reaction network of the model. Note in particular the reaction in which contact between I_0 and S , mediated by mutant virions v_1 (with transmission rate β_{01}), results in an individual that is neither infected nor susceptible, *i.e.*, belonging to the recovered class R . The microscopic component remains unchanged, except that $\tilde{f}_1 = 0$ as $I_1 \rightarrow 0$, implying that no substrate is available for mutant replication.

large a_1), and slow recovery at the population level (effectively small π_1). Each example exhibits the core macroscopic level signature reproduced by our model: rapid epidemic growth, high mortality, and self-limitation throughout host depletion or behavioral change, sometimes followed by longer-term evolutionary relaxation.

Firstly, the introduction of myxoma virus (MYXV) into Australia to control invasive European rabbits provides a classic illustration [35]. Initial mortality reached approximately 99 %, and MYXV spread explosively via arthropod vectors, collapsing rabbit populations from an estimated ~ 600 million to ~ 100 million within a few years, a textbook burnout pulse (huge realized a_1 in a highly connected host–vector system combined with extreme δ_1). Remarkably, subsequent coevolution reduced virulence and increased host resistance, gradually shifting the system away from the burnout regime [36]. Secondly, the 2014–2016 West African outbreak of Zaire Ebolavirus (ZEBOV) was the largest filovirus outbreak on record, with estimated case fatality rates around 60 - 70 % [37]. Simple growth models during early spread gave $R_0 \approx 1.6 - 2.0$, indicating sustained human-to-human transmission [38]. These outbreaks typically burn out once susceptible depletion, improved infection prevention, and control reduce effective transmission, consistent with a high δ_1 process that self-limits in the absence of continuous replenishment of susceptibles. Thirdly, since 2021 – 2023, highly pathogenic avian influenza virus (HPAIV) H5N1 clade 2.3.4.4b has caused unprecedented die-offs in wild birds and mass mortality in marine mammals [39]. These events reveal intense transmission in dense breeding colonies coupled with extremely high mortality, exemplifying the “ignite fast, die fast” pattern. Genomic epidemiology provides evidence consistent with mammal-to-mammal transmission in pinnipeds. In such colonies, the realized a_1 becomes very large while δ_1 is extreme, leading to rapid exhaustion of susceptible and epizootic burnout [40].

To explore the evolutionary consequences of virulence emergence, we devote this section to analyzing a scenario in which an initially avirulent master strain ($\delta_0 = 0$) with moderate transmission ($a_0 = 2$) gives rise to a mutant variant with higher virulence and transmissibility, here $\delta_1 = 1$ and $a_1 = 3$. All the remaining parameters of the model have been conveniently fixed at the following values:

$$\begin{aligned} \chi &= 2, & \delta_0 &= 0, & \delta_1 &= 1, & \pi_0 &= \pi_1 = 0.2, & a_0 &= 2, & a_1 &= 3, & b_0 &= b_1 = 0.5, \\ f_0 &= 1, & f_1 &= 0.1, & \gamma_0 &= \gamma_1 = 0.5, & \xi_0 &= \xi_1 = 3, & \gamma_0 &= 0.8. \end{aligned} \quad (24)$$

Again, the slow-fast time ratio is taken as $\varepsilon = 0.01$.

As a first step in this study, we vary the mutation probability μ and analyze its impact on the dynamics of the system. In particular, we monitor: (i) the evolution of the state variables; (ii) the effective transmission rates of both strains (β_{00} , β_{01} , and β_{11}); and (iii) the instantaneous fitness of each variant (\tilde{f}_0 and \tilde{f}_1) and the dynamic critical mutation threshold ($\mu_c = \mu_c(t)$), both characteristics being crucial in the inter-level connection. Three snapshots of this analysis are shown in Figure 10.

We highlight the particularly interesting case arising in the central panels of Figure 10, where the master variant appears to overcome a pseudo-error catastrophe. This abrupt transition arises due to the micro– to macroscopic coupling inherent in the model.

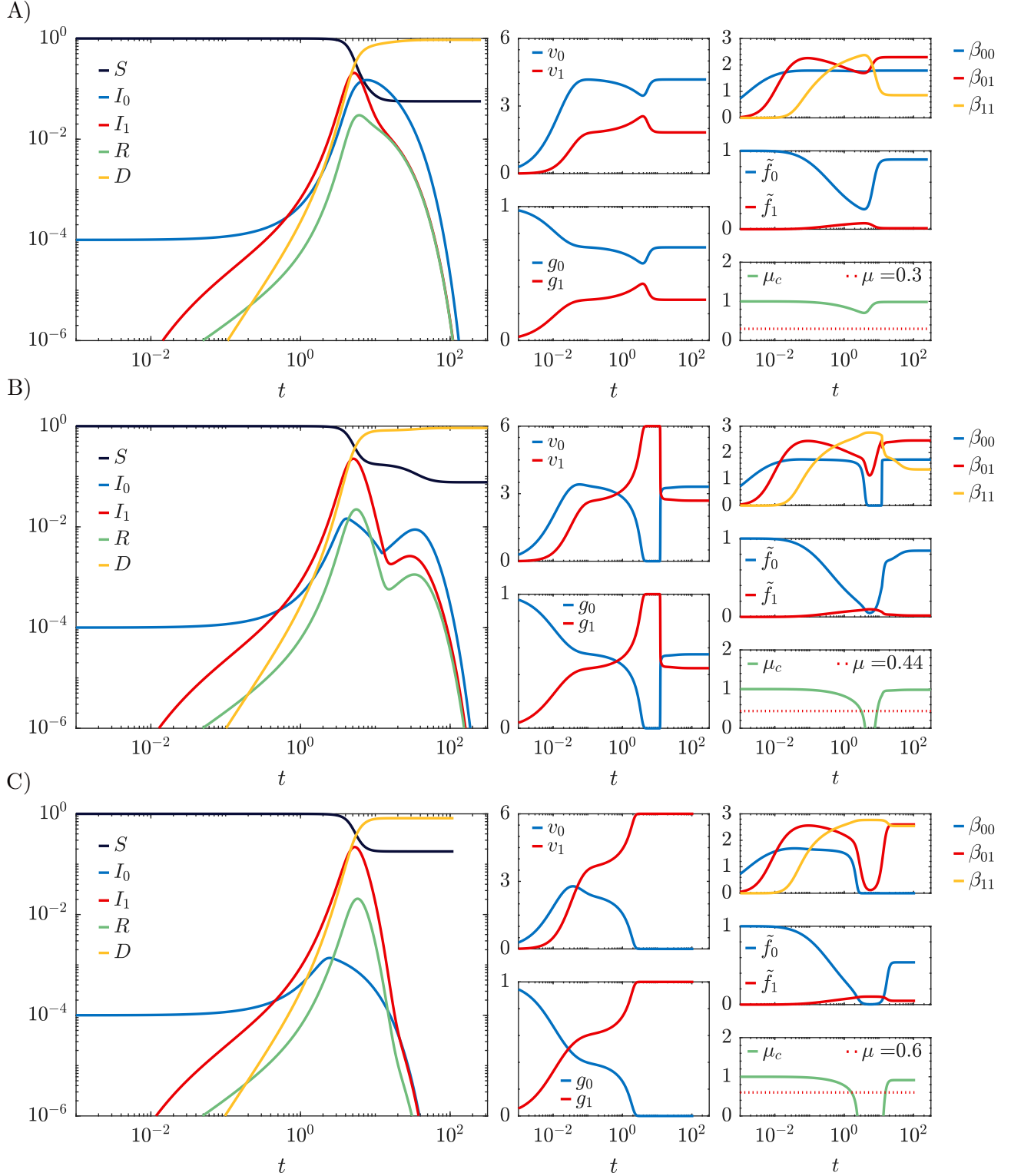


Figure 10: Numerical integrations of the system for non-varying parameter set (24). The slow to fast time ratio is fixed at $\varepsilon = 0.01$. To avoid false recoveries from pseudo-extinction, we set to zero any variable below the numerical tolerance of the ODE numerical integrator (*i.e.* 10^{-14}).

When the mutation probability is very high (*e.g.*, $\mu \gtrsim 0.4$), continuous generation of mutant genomes g_1 drives a rapid rise in virions v_1 , which boosts the strain-specific transmission rate and shifts prevalence so that $I_1 \gg I_0$. This macroscopic level shift depresses the master's context-dependent error threshold $\mu_c(t)$, pushing

the within-host quasispecies beyond the threshold and causing a transient microscopic pseudo-extinction of g_0 , a behavior consistent with error-catastrophe experiments in poliovirus exposed to ribavirin [19]. Because the mutant is highly virulent $\delta_1 \gg 0$, mortality rapidly depletes I_1 , transmission collapses, and conditions that favor the master return: as g_1 declines, the master's effective replicative fitness \tilde{f}_0 increases, $\mu_c(t)$ rises above μ , and residual g_0 genomes can resume replication. A macroscopic scale analogue of this "ignite fast, die fast" endgame appears in the aforementioned HPAIV wildlife pulses, where explosive spread with extreme lethality in dense colonies (e.g., sea lion mass mortality in Peru) is followed by rapid chain collapse [40]. Ultimately, the epidemic wanes as cumulative deaths disrupt infection chains; in our parameter region with $\delta_0 = 0$ and $\delta_1 > 0$, only disease-free equilibria (DFE) are feasible, and numerical simulations show the principal trajectory converges to DFE across comparable parameter sets. We analyze the DFE behavior as a function of μ for the representative parameter choice given in (24).

- **Disease-free equilibria (DFE).** From Proposition 1, they are of the form:

$$(S, I_0, I_1, R, D) \times (g_0, g_1; v_0, v_1) = (S^*, 0, 0, 0, 1 - S^*) \times \left(g_0^*, 1 - g_0^*; \frac{g_0^* \xi_0}{\gamma_0}, \frac{(1 - g_0^*) \xi_1}{\gamma_1} \right).$$

These DFE equilibria fill a 2-dimensional plane, governed by the variables (S^*, g_0) . Their local stability can be approached by their linearised system. Indeed, the spectrum of the corresponding jacobian matrices is given by

$$\lambda_{\text{DFE}} = \{0, 0, 0, 0, -\chi, -\gamma_0, -\gamma_1, -(\delta_1 + \pi_1), \psi(S^*, g_0^*)\}.$$

where

$$\psi(S^*, g_0^*) = \frac{a_0 \xi_0 g_0^* S^*}{b_0 \gamma_0 + \xi_0 g_0^*} - \pi_0.$$

The four zero eigenvalues come from the first integrals $I_0 = 0$, $I_1 = 0$, $R = 0$, and $S + I_0 + I_1 + R + D = 1$. There are four more negative eigenvalues and a last one, $\psi(S^*, g_0^*)$, whose sign determines their (transversal) stability. Indeed, $\psi(S^*, g_0^*) = 0$ is equivalent to the hyperbola (see Figure 11).

$$S^* = \frac{\pi_0}{a_0} \left(1 + \frac{b_0 \gamma_0}{\xi_0} \frac{1}{g_0^*} \right), \quad g_0^* \in (0, 1]. \quad (25)$$

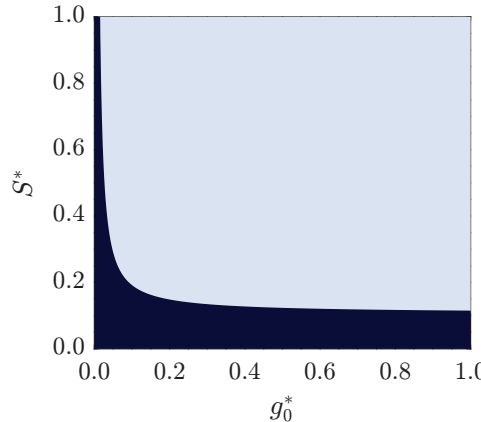


Figure 11: Stability regions of the DFE plane. The attractive (unstable) region of each DFE point is represented in black (grey) colour, in terms of g_0^* and S^* . The hyperbola $\psi(S^*, g_0^*) = 0$ dividing both zones is given by (25).

4 Discussion

We have presented a minimal, mechanistically grounded multiscale framework that links within-host quasispecies dynamics to population-level SIRS epidemiology through explicit, bidirectional coupling: transmission rates β_{ij}

depend on the instantaneous virion abundance $v_j(t)$ (microscopic to macroscopic), and the effective replicative rates \tilde{f}_j are weighted by the prevalence of each infected host class (macroscopic to microscopic). The imposed slow-fast structure ($\varepsilon \ll 1$) yields a natural quasi-steady reduction of the genome-virion subsystem and explains why, on epidemiological timescales, transmission can be treated as time-varying process inherited from the fast layer while preserving a conserved quasispecies backbone. This construction moves beyond *ad hoc* scale-bridging approaches by keeping the error-threshold mechanism explicit and intrinsically context-dependent.

Our NGM calculation at DFE yields $\mathcal{R}_0 = \max \{\beta_{00}/(\pi_0 + \delta_0), \beta_{11}/(\pi_1 + \delta_1)\}$, clarifying that the cross-seeding pathway β_{01} does not affect invasion, because the jacobian block is triangular at DFE (no mutant virions are present). In contrast, β_{01} plays a crucial role after invasion: once any $I_0 > 0$ exists, the β_{01} channel accelerates mutant establishment and shapes transient dynamics of strain replacement. The slow-fast closure further justifies the introduction of time-dependent effective reproduction numbers $\mathcal{R}_t^{(0)}$ and $\mathcal{R}_t^{(1)}$, and the growth diagnostic $\mathcal{G}_t > 0$ (see (18)) that decomposes overall expansion into outflow-weighted excess reproduction of each strain (Section 3.3). These quantities admit clear biological interpretation and naturally connect to empirical data through longitudinal proxies of viral load $v_j(t)$, which control the saturating transmission functions β_{ij} .

A central theoretical contribution of this work is the demonstration that the error threshold becomes epidemic-state dependent (see (4)). As a transmissible mutant rises in prevalence (ν decreases), the critical mutation rare $\mu_c(\nu)$ decreases, so that, at fixed polymerase fidelity, the master g_0 can transiently fall below its error threshold. This produces a pseudo-error catastrophe driven by cross-scale feedback rather than a biochemical change in replication fidelity (Section 3.5; central panel of Figure 10). As mortality and host depletion subsequently collapse I_1 , $\mu_c(\nu)$ increases again above μ , allowing residual g_0 to resume replication, thereby explaining the observed “disappear-then-reappear” microscopic signature during a macroscopic burnout pulse. This mechanism cannot be recovered when within- and between-host scales are analyzed in isolation.

The model yields sharp feasibility inequalities that delineate endpoints and coexistence regimes. For example, at candidate coexistence one obtains the condition $\pi_0 \beta_{00}^* < \pi_1 \beta_{11}^*$ (Section 3.1), where starred quantities denote the quasi-steady transmission rates inherited from the fast layer. Because β_{ij}^* retain hyperbolic saturation and depend explicitly on (ξ_j, γ_j, f_j) , these inequalities make transparent how within-host production efficiencies bias population-level toward coexistence, no master or disease-free endpoints.

Linear stability analysis reveals complex conjugate eigenvalues for NME and CSE across broad parameter regions (Figures 6 and 8), predicting damped oscillations in I_0, I_1 and g_j, v_j , even in the absence of external forcing, a distinctive dynamical signature of the multiscale feedback. The quasi-period near NME follows directly from this complex eigenvalue pair (see (22) and Figure 7).

Two illustrative regimes bracket the model’s behavior and directly connect to well-documented biology. In the “vaccine-like” quadrant ($\delta_0 = \delta_1 = 0, \pi_1 \gg \pi_0$), the mutant benignly replaces and persists at appreciable prevalence, generating high seroprevalence without excess mortality (Section 3.4; Figure 3), consistent with live attenuated, strongly immunizing circulation. In the “burnout” quadrant ($\delta_1 \gg 0$, modest or weak π_1), a hypervirulent mutant self-limits throughout host depletion: the epidemic surge can pass through a pseudo-extinction of g_0 before collapsing back to the DFE, as observed numerically across a wide range of mutation rates (Section 3.5 and Figure 10). Together, these extremes emphasize that epidemic composition, rather than intrinsic polymerase fidelity alone, governs transient excursions across error thresholds.

We can also draw several practical implications from our study. (i) Transient sequencing signatures: during mutant ascents, we predict a temporary loss of the master sequence in within-host spectra, coupled to peaks in incidence, interpretable as a population-driven passage through the threshold $\mu_c(\nu)$. (ii) Oscillatory returns: damped endemic waves should arise where the two-strain slow system has complex eigenvalues; these oscillations can be quantitatively fitted with virion-dependent transmission functions β_{ij} applied to joint incidence and viral load time series. (iii) Design criteria for benign replacement: the coexistence inequalities translate empirically measured load-transmission curves (a_j, b_j) and immune induction (π_1) into operational thresholds for safe dominance.

We intentionally compressed within-host diversity into a two-type, unidirectional quasispecies and neglect explicit immune kinetics, host heterogeneity, demographic turnover (births and immigration of susceptibles), contact structure, and stochastic fade-out. These simplifying choices enable analytical tractability but preclude

phenomena such as diversification fronts, antigenic escape, and age or network effects on epidemic thresholds. The explicit slow-fast structure of the model suggests a rigorous Tikhonov reduction to a closed slow system, a global bifurcation analysis (saddle-node, Hopf) expressed in terms of measurable parameters (*e.g.*, peak viral load and decay), and extensions incorporating reverse mutation, multi-lineage competition, host heterogeneity in susceptibility and waning immunity, and stochastic invasion dynamics. Finally, the $\pi_1 \rightarrow \infty$ limit (Section 3.4.3) motivates the study of defective viral genomes within the same multiscale closure, in which the cross-seeding pathway β_{01} functions as an “immunizing contact” that induces host immunity without productive mutant infection.

5 Concluding remarks

By tying transmission directly to intracellular production and allowing epidemiological prevalence to feedback on effective replication, our model shows how selection pressures at one scale can induce phase transition-like shifts at the other. Most notably, how a mutant surge can transiently trigger an intrahost error catastrophe and how extreme virulence self-limits transmission and spread. The “vaccine-like” and “burnout” regimes bracket a continuum of realistic outcomes, unify microscopical and macroscopic thresholds (from $\mu_c(\nu)$ to \mathcal{R}_0), and yield testable signatures in coupled incidence–viral-load time series. We anticipate that combining quasi-steady reductions, joint inference on $\beta_{ij}(v_j)$ from viral load and contact data, and explicit heterogeneity will transform this conceptual bridge into a practical tool for anticipating which mutants are poised to dominate, coexist, or extinguish themselves—and why.

6 Acknowledgements

JCM-S was supported by Generalitat Valenciana grant ACIF/2021/296. JTL and JS thank the AEI, through the María de Maeztu Program for Units of Excellence in R&D (CEX2020-001084-M) and the Generalitat de Catalunya CERCA Program for institutional support. JTL has been also funded by grants PID2021-122954NB-I00 and PID2024-155942NB-I00 funded by MICIU/AEI/10.13039/501100011033 and “ERDF a way of making Europe”. SFE was supported by grants PID2022-136912NB-I00 funded by MICIU/AEI/10.13039/501100011033 and by “ERDF a way of making Europe”, and CIPROM/2022/59 funded by Generalitat Valenciana. JCM-S, JTL and SFE thank support from the Santa Fe Institute.

References

- [1] Shuhua Mi, Xiangdong Lee, Xian-Yang Li, Gail M. Veldman, Helen Finnerty, Leslie Racie, Elizabeth LaVallie, Xu-Yong Tang, Patrick Edouard, Stephen Howes, Michael Keith, and James M. McCoy. Syncytin is a captive retroviral envelope protein involved in human placental morphogenesis. *Nature*, 403:785–789, 2000.
- [2] B. Jesse Shapiro and Paul E. Turner. Evolution of mutualism from parasite–host interactions. *Evolution*, 72(6):1274–1285, 2018.
- [3] Julien Doumayrou, Anouk Avellan, Rémi Froissart, and Yannis Michalakis. An experimental test of the transmission–virulence trade-off hypothesis in a plant virus. *Evolution*, 67(2):477–486, 2013.
- [4] Ricard Solé, Josep Sardanyés, and Santiago F. Elena. Phase transitions in virology. *Reports on Progress in Physics*, 84(11):115901, 2021.
- [5] Manfred Eigen. Selforganization of matter and the evolution of biological macromolecules. *Naturwissenschaften*, 58(10):465–523, 1971.
- [6] Manfred Eigen, John McCaskill, and Peter Schuster. The molecular quasi-species. In Ilya Prigogine and Stuart A. Rice, editors, *Advances in Chemical Physics*, volume 75, pages 149–263. John Wiley & Sons, 1989.

- [7] Marc Barthélémy, Alain Barrat, Romualdo Pastor-Satorras, and Alessandro Vespignani. Dynamical patterns of epidemic outbreaks in complex heterogeneous networks. *Journal of Theoretical Biology*, 235(2):275–288, 2005.
- [8] Duygu Balcan and Alessandro Vespignani. Phase transitions in contagion processes mediated by recurrent mobility patterns. *Nature Physics*, 7:581–586, 2011.
- [9] Daniel Coombs, Michael A. Gilchrist, and Christina L. Ball. Evaluating the importance of within- and between-host selection pressures on the evolution of chronic pathogens. *Theoretical Population Biology*, 72(4):576–591, 2007.
- [10] Nicole Mideo, Samuel Alizon, and Troy Day. Linking within- and between-host dynamics in the evolutionary epidemiology of infectious diseases. *Trends in Ecology & Evolution*, 23(9):511–517, 2008.
- [11] Zhilan Feng, Jorge X. Velasco-Hernández, Beatriz Tapia-Santos, and Maria C. A. Leite. A model for coupling within-host and between-host dynamics in an infectious disease. *Nonlinear Dynamics*, 68:401–411, 2012.
- [12] Stephanie O. Scholle, Rianne J. F. Ypma, Alun L. Lloyd, and Katia Koelle. Viral substitution rate variation can arise from the interplay between within-host and epidemiological dynamics. *The American Naturalist*, 182(4):494–513, 2013.
- [13] Jeewoen Shin and Thomas MacCarthy. Potential for evolution of complex defense strategies in a multi-scale model of virus-host coevolution. *BMC Evolutionary Biology*, 16:233, 2016.
- [14] Hilje M. Doekes, Nicole Mideo, and Franz J. Weissing. Theory for the evolution of virulence in generalist pathogens: The role of host heterogeneity. *The American Naturalist*, 190(6):E193–E207, 2017.
- [15] Narges Dorratoltaj, Nikhil M. Marathe, Pinar Keskinocak, Julie S. Swann, and Bariş M. Koçaga. A systematic review of within-host and between-host models of infectious diseases. *PeerJ*, 5:e3877, 2017.
- [16] Josep Sardanyés and Santiago F. Elena. Quasispecies spatial models for RNA viruses with different replication modes and infection strategies. *PLoS ONE*, 6:e24884, 2011.
- [17] Fabiola S. Heldt, Theresia Frensing, and Udo Reichl. Modeling the intracellular dynamics of influenza virus replication to understand the control of viral growth. *PLoS Computational Biology*, 9(11):e1003372, 2013.
- [18] Philipp Kumberger, Frederik Frederiksen, Michael G. Schwarz, Johannes Köster, and Vahid Sandoghdar. Multiscale modeling of virus replication and spread. *FEBS Letters*, 590(12):1972–1984, 2016.
- [19] Seán Crotty, Craig E. Cameron, and Raul Andino. RNA virus error catastrophe: Direct molecular test by using ribavirin. *Proceedings of the National Academy of Sciences of the United States of America*, 98(12):6895–6900, 2001.
- [20] Ricard V. Solé, Josep Sardanyés, Juana Díez, and Antonio Mas. Information catastrophe in RNA viruses through replication thresholds. *Journal of Theoretical Biology*, 240(3):353–359, 2006.
- [21] Alberto M. Carabelli, Thomas P. Peacock, Luke G. Thorne, William T. Harvey, Joseph Hughes, COVID-19 Genomics UK Consortium, Sharon J. Peacock, Wendy S. Barclay, Thushan I. de Silva, Greg J. Towers, and David L. Robertson. SARS-CoV-2 variant biology: Immune escape, transmission and fitness. *Nature Reviews Microbiology*, 21(3):162–177, 2023.
- [22] Ricard V. Solé. Phase transitions in unstable cancer cell populations. *The European Physical Journal B*, 35(1):117–123, 2003.
- [23] J. Swetina and Peter Schuster. Self-replication with errors: A model for polynucleotide replication. *Biochemical Chemistry*, 16(4):329–345, 1982.
- [24] Herbert W. Hethcote. The mathematics of infectious diseases. *SIAM Review*, 42(4):599–653, 2000.
- [25] Odo Diekmann and Johan Andreas Petrus Heesterbeek. *Mathematical epidemiology of infectious diseases: model building, analysis and interpretation*. John Wiley & Sons, Chichester, West Sussex, England, 2000.

[26] Pauline van den Driessche and James Watmough. Reproduction numbers and sub-threshold endemic equilibria for compartmental models of disease transmission. *Mathematical Biosciences*, 180:29–48, 2002.

[27] Pauline van den Driessche and James Watmough. Further notes on the basic reproduction number. In Fred Brauer, Pauline van den Driessche, and Jianhong Wu, editors, *Mathematical Epidemiology*, volume 1945 of *Lecture Notes in Mathematics*, pages 159–178. Springer, Berlin, Heidelberg, 2008.

[28] Grace R. Macklin, Corey Peak, Martin Eisenhawer, Feyrouz Kurji, Ondrej Mach, John Konz, Chris Gast, Novilia Sjafri Bachtiar, Ananda S. Bandyopadhyay, and Simona Zipursky. Enabling accelerated vaccine rollout for public health emergencies of international concern (pheics): novel oral polio vaccine type 2 (nOPV2) experience. *Vaccine*, 41(Supplement 1):A122–A127, 2023. on behalf of the nOPV2 Working Group.

[29] Chris Gast, Ananda S. Bandyopadhyay, Xavier Sáez-Llorens, Teresita de Leon, Rodolfo DeAntonio, Jose Jimeno, Gonzalo Aguirre, Lisa M. McDuffie, Emily Coffee, David L. Mathis, Mark S. Oberste, William C. Weldon, Jennifer L. Konopka-Anstadt, John Modlin, Novilia Sjafri Bachtiar, Andrea Fix, John Konz, Robert Clemens, S. A. Costa Clemens, and Roger Rüttimann. Fecal shedding of 2 novel live attenuated oral poliovirus type 2 vaccine candidates by healthy infants administered bivalent oral poliovirus vaccine/inactivated poliovirus vaccine: 2 randomized clinical trials. *The Journal of Infectious Diseases*, 226(5):852–861, 2022.

[30] Carlos F. Estivariz, Steve D. Kovacs, and Ondrej Mach. Review of use of inactivated poliovirus vaccine in campaigns to control type 2 circulating vaccine derived poliovirus (cVDPV) outbreaks. *Vaccine*, 41(1):A113–A121, 2023.

[31] Bo Zhou and Wen Niu. Efficacy of live oral rotavirus vaccines. *The Lancet Infectious Diseases*, 19(9):929, 2019.

[32] Matthew A. Zalot, Michael M. Cortese, Kathleen P. O’Callaghan, Meaghan C. Casey-Moore, Nicole L’Etoile, S. Leeann Smart, Michael J. Honeywood, Srdjan Mijatovic-Rustempasic, Jacqueline E. Tate, Alyssa Davis, Nicole Wittmeyer, Catherine McGann, Shazia Sadaf, Kristin Wilson, Michael D. Bowen, Rashi Gautam, Umesh D. Parashar, Susan E. Coffin, and Kimberly A. Gibbs. Risk of transmission of vaccine-strain rotavirus in a neonatal intensive care unit that routinely vaccinates. *Pediatrics*, 155(1):e2024067621, 2025.

[33] Marco Vignuzzi and Carolina B. López. Defective viral genomes are key drivers of the virus–host interaction. *Nature Microbiology*, 4(7):1075–1087, 2019.

[34] Thomas Notton, Josep Sardanyés, and Leor S. Weinberger. The case for transmissible antivirals to control population-wide infectious disease. *Trends in Biotechnology*, 32(8):400–405, 2014.

[35] Peter J. Kerr, Isabella M. Cattadori, Jing Liu, David G. Sim, Jason W. Dodds, James W. Brooks, Michael J. Kennett, Edward C. Holmes, and Andrew F. Read. Evolutionary history and attenuation of myxoma virus on two continents. *PLoS Pathogens*, 8(10):e1002950, 2012.

[36] Peter J. Kerr, Matthew B. Rogers, Adam Fitch, Jay V. Depasse, Isabella M. Cattadori, Alan C. Twaddle, Peter J. Hudson, David C. Tscharke, Andrew F. Read, Edward C. Holmes, and Elodie Ghedin. Genome-scale evolution of myxoma virus reveals host–pathogen adaptation and rapid geographic spread. *Journal of Virology*, 87(23):12900–12915, 2013.

[37] Adam J. Kucharski and W. John Edmunds. Case fatality rate for Ebola virus disease in West Africa. *The Lancet*, 384(9950):1260, 2014.

[38] Christian L. Althaus. Rapid drop in the reproduction number during the Ebola outbreak in the Democratic Republic of Congo. *PeerJ*, 3:e1418, 2015.

[39] Mariana Leguia, Alejandra Garcia-Glaessner, Breno Muñoz-Saavedra, Diana Juarez, Patricia Barrera, Carlos Calvo-Mac, Javier Jara, Walter Silva, Karl Ploog, Lady Amaro, Paulo Colchao-Claux, Christine K. Johnson, Marcela M. Uhart, Martha I. Nelson, and Jesus Lescano. Highly pathogenic avian influenza A (H5N1) in marine mammals and seabirds in Peru. *Nature Communications*, 14:5489, 2023.

- [40] Víctor Gamarra-Toledo, Pablo I. Plaza, Roberto Gutiérrez, Giancarlo Inga-Díaz, Patricia Saravia-Guevara, Oliver Pereyra-Meza, Elver Coronado-Flores, Antonio Calderón-Cerrón, Gonzalo Quiroz-Jiménez, Paola Martínez, Deyvis Huamán-Mendoza, José C. Nieto-Navarrete, Sandra Ventura, and Sergio A. Lambertucci. Mass mortality of sea lions caused by highly pathogenic avian influenza A(H5N1) virus. *Emerging Infectious Diseases*, 29(12), 2023.
- [41] Manfred Eigen and Peter Schuster. A principle of natural self-organization. part A: Emergence of the hypercycle. *Naturwissenschaften*, 64(11):541–565, 1977.

APPENDIX

A Equilibrium points: proofs of the propositions

A.1 Proof of Lemma 1

Notice that if one defines $\tilde{f}_0 = f_0\nu^*$ and $\tilde{f}_1 = f_1\nu^*$, the microscopic system becomes

$$\varepsilon\dot{g}_0 = \tilde{f}_0(1 - \mu)g_0 - \Phi g_0, \quad \varepsilon\dot{g}_1 = \tilde{f}_0\mu g_0 + \tilde{f}_1 g_1 - \Phi g_1,$$

with $\Phi = \tilde{f}_0g_0 + \tilde{f}_1g_1$. This is a standard quasispecies model with fitnesses \tilde{f}_0 and \tilde{f}_1 . It is well-known [41] that there are two possible scenarios for its equilibrium points in terms of the relation between the mutation probability μ and the corresponding critical mutation probability.

$$\mu_c^* = 1 - \frac{\tilde{f}_1}{\tilde{f}_0} = 1 - \frac{f_1}{f_0} \left(\frac{1}{\nu^*} - 1 \right).$$

(i) If $0 < \mu < \mu_c^*$ then the equilibrium point is

$$(g_0^*, g_1^*) = \left(1 - \frac{\mu}{\mu_c^*}, \frac{\mu}{\mu_c^*} \right).$$

(ii) On the contrary, if $\mu_c^* \leq \mu \leq 1$, the equilibrium point is uniquely composed by mutant genomes: $(g_0^*, g_1^*) = (0, 1)$.

The expressions for the equilibrium virions derive straightforwardly from the ones for the genomes. □

A.2 Proof of Proposition 1 (DFE)

Under the assumption $I_0^* = I_1^* = 0$ the macroscopic system becomes

$$\dot{S} = \chi R, \quad \dot{I}_0 = 0, \quad \dot{I}_1 = 0, \quad \dot{R} = -\chi R, \quad \dot{D} = 0.$$

Equating them to zero (to seek for equilibrium points) we get $R^* = 0$ if $\chi \neq 0$ or arbitrary R when $\chi = 0$. Regarding the microscopic system, since $I_0^* = I_1^* = 0 \Rightarrow \nu_0^* = \nu_1^* = 0$ we have $\tilde{f}_0 = \tilde{f}_1 = \Phi = 0$ and so

$$\varepsilon\dot{g}_0 = 0, \quad \varepsilon\dot{g}_1 = 0,$$

which leads to equilibria with arbitrary (g_0, g_1) such that $g_0 + g_1 = 1$. Regarding virions, it is straightforward to show that the equilibria are of type

$$v_0 = \frac{\xi_0}{\gamma_0}g_0, \quad v_1 = \frac{\xi_1}{\gamma_1}g_1,$$

for any (g_0, g_1) satisfying $g_0 + g_1 = 1$. □

A.3 Proof of Proposition 2 (NME)

Substituting $I_0^* = 0$ in $\dot{D} = \delta_0 I_0^* + \delta_1 I_1^* = 0$ it turns out that $\delta_1 I_1^* = 0$. Since $I_1^* > 0$ it follows that, necessarily, $\delta_1 = 0$. We consider two cases:

(i) Case $\beta_{11} > 0$. This is divided, in its turn, into:

(i₁) Case $\chi > 0$. From $\nu^* = 0$ we have, in particular, that $\beta_{01} = 0$. Substituting $I_0^* = 0$ into (9), $\dot{I}_1 = 0$, we obtain

$$(\beta_{11}S - (\pi_1 + \delta_1))I_1 = 0 \Rightarrow S = \frac{\pi_1 + \delta_1}{\beta_{11}},$$

which becomes

$$S^* = \frac{\pi_1}{\beta_{11}}.$$

since $\delta_1 = 0$. Substituting now $I_0 = 0$ into (10) we get

$$\dot{R} = \pi_1 I_1 - \chi R = 0 \Rightarrow R^* = \frac{\pi_1}{\chi} I_1,$$

which is well defined since $\chi > 0$. The variable D^* is defined such that $S^* + I_1 + R^* + D^* = 1$.

(i₂) Case $\chi = 0$: we have, from the same argument as above, that $S^* = \pi_1 / \beta_{11}$. However,

$$\dot{R} = 0 \Leftrightarrow \pi_1 I_1^* = 0 \Rightarrow \pi_1 = 0 \Rightarrow S^* = 0.$$

That is, in this scenario, necessarily $\pi_1 = 0$ and the equilibrium point for the macroscopic system is of the form $(S^*, I_0^*, I_1^*, R, D) = (0, 0, I_1, R, D)$ with arbitrary R, D , such that $I_1^* + R + D = 1$.

(ii) Case $\beta_{11} = 0$: the conditions for having an equilibrium point reduce to $\chi R = 0$ and $-\pi_1 I_1^* = 0$. From the second equation it follows that, necessarily, $\pi_1 = 0$. From the first one, we have two possible solutions:

(ii₁) If $\chi > 0$: then $R^* = 0$ and the point are of the form $(S, I_0^*, I_1^*, R^*, D) = (S, 0, I_1, 0, D)$ with arbitrary S and D satisfying that $S + I_1^* + D = 1$.

(ii₂) If $\chi = 0$: the equilibrium is of the form $(S, I_0^*, I_1^*, R, D) = (S, 0, I_1, R, D)$ with arbitrary R, S and D such that $S + I_1^* + R + D = 1$.

In both two cases (i) and (ii), at the genome's level, $\nu^* = 0$ translates into $\Phi = f_1 g_1$ and so

$$\varepsilon \dot{g}_0 = -\Phi g_0 = -f_1 g_1 g_0 = 0, \quad \varepsilon \dot{g}_1 = f_1 g_1 - \Phi g_1 = f_1 g_1 (1 - g_1) = 0.$$

Since $g_0 + g_1 = 1$ the only two solutions of the latter equations is either $(g_0^*, g_1^*) = (1, 0)$ or $(g_0^*, g_1^*) = (0, 1)$. Therefore, joint to the corresponding solutions for the virion's system, one obtains the following two possible equilibrium points for the microscopic system:

$$\text{QS}_{\text{mic}}^{(0)} : (g_0^*, g_1^*; v_0^*, v_1^*) = \left(1, 0, \frac{\xi_0}{\gamma_0}, 0\right) \quad \text{and} \quad \text{QS}_{\text{mic}}^{(1)} : (g_0^*, g_1^*; v_0^*, v_1^*) = \left(0, 1, 0, \frac{\xi_1}{\gamma_1}\right).$$

For $\text{QS}_{\text{mic}}^{(1)}$ the condition $\beta_{11} = 0$ implies that either $a_1 = 0$ or $\xi_1 = 0$. \square

A.4 Proof of Proposition 3 (NmutE)

Let us start computing the possible equilibrium points of the microscopic system. Indeed, $I_1^* = 0 \Rightarrow \nu^* = 1 \Rightarrow \Phi = f_0 g_0$. Thus, the equilibrium points of the genome's system must solve

$$\begin{aligned}\varepsilon \dot{g}_0 &= f_0(1 - \mu)g_0 - (f_0 g_0)g_0 = f_0 g_0(1 - \mu - g_0) = 0 \\ \varepsilon \dot{g}_1 &= f_0 \mu g_0 - (f_0 g_0)g_1 = f_0 g_0(\mu - g_1) = 0.\end{aligned}$$

Since $f_0 > 0$ they become

$$g_0(1 - \mu - g_0) = 0 \quad \text{and} \quad g_0(\mu - g_1) = 0,$$

which leads to two possible cases depending on g_0 vanishing or not. Thus,

(a) Case $g_0 = 0$: so $g_1 = 1$ and then $(g_0^*, g_1^*) = (0, 1)$. Regarding the virion's system, it becomes

$$\begin{aligned}\varepsilon \dot{v}_0 &= \xi_0 g_0^* - \gamma_0 v_0 = -\gamma_0 v_0 = 0 \Rightarrow v_0^* = 0. \\ \varepsilon \dot{v}_1 &= \xi_1 g_1^* - \gamma_1 v_1 = \xi_1 - \gamma_1 v_1 = 0 \Rightarrow v_1^* = \frac{\xi_1}{\gamma_1}.\end{aligned}$$

So, the equilibrium point is

$$(g_0^*, g_1^*; v_0^*, v_1^*) = \left(0, 1, 0, \frac{\xi_1}{\gamma_1}\right) =: \text{QS}_{\text{mic}}^{(1)}.$$

Notice that $v_0^* = 0$ implies that $\beta_{00}^* = 0$ and from $\nu^* = 1$ it follows that $\beta_{11}^* = 0$.

(b) Case $g_0 \neq 0$: this implies $(g_0^*, g_1^*) = (1 - \mu, \mu)$ with $0 < \mu < 1$. Again, substituting into the virion's system we get

$$\begin{aligned}\varepsilon \dot{v}_0 &= \xi_0 g_0^* - \gamma_0 v_0 = 0 \Rightarrow v_0^* = \frac{\xi_0}{\gamma_0}(1 - \mu), \\ \varepsilon \dot{v}_1 &= \xi_1 g_1^* - \gamma_1 v_1 = 0 \Rightarrow v_1^* = \frac{\xi_1}{\gamma_1}\mu.\end{aligned}$$

So, the equilibrium point for the microscopic system is

$$(g_0^*, g_1^*; v_0^*, v_1^*) = \left(1 - \mu, \mu, \frac{\xi_0}{\gamma_0}(1 - \mu), \frac{\xi_1}{\gamma_1}\mu\right) =: \text{QS}_{\text{mic}}^{(\mu)}. \quad (\text{A1})$$

Moreover, $\beta_{11} = 0$ (since $\nu^* = 1$) and

$$\beta_{00}^* = \frac{a_0 v_0^*}{b_0 + v_0^*}, \quad \beta_{01}^* = \frac{a_1 v_1^*}{b_1 + v_1^*},$$

which vanish if and only if $a_0 = 0$ or $v_0^* = 0$ and $a_1 = 0$ or $v_1^* = 0$, respectively.

Having in mind these two equilibria for the microscopic system, we seek the equilibrium points of the macroscopic system. From the assumptions $I_0^* \neq 0$ and $I_1^* = 0$, the macroscopic equations $\dot{S} = 0, \dot{I}_j = 0, \dot{R} = 0, \dot{D} = 0$ ($j = 0, 1$) become

$$(\beta_{00} + \beta_{01}) I_0^* S = \chi R, \quad (\text{A2})$$

$$(\beta_{00} S - (\pi_0 + \delta_0)) I_0^* = 0,$$

$$\beta_{01} I_0^* S = 0,$$

$$\chi R = \pi_0 I_0^*, \quad (\text{A3})$$

$$\delta_0 I_0^* = 0, \quad (\text{A4})$$

where it has been taken into account that $I_1^* = 0$ implies $\nu^* = 1$. From (A4) it is clear that a necessary condition to have an equilibrium of such type is that $\delta_0 = 0$. In the following, this will be assumed.

To analyze it we discuss two cases: $\chi > 0$ and $\chi = 0$. Precisely,

(i) Case $\chi > 0$: In this scenario and using that $I_0^* > 0$, equations (A2)-(A3) become

$$(\beta_{00} + \beta_{01})I_0^*S = \chi R, \quad \beta_{00}S = \pi_0, \quad \beta_{01}S = 0, \quad \chi R = \pi_0I_0^*.$$

From here we have four possible scenarios:

(i₁) Case $\beta_{00} = 0$ and $\beta_{01} > 0$: second and third equation requires π_0 and $S^* = 0$ respectively. Given this result the first and last equation result into $R^* = 0$. With this, the equilibrium reads as

$$(S^*, I_0^*, I_1^*, R^*, D^*) = (0, I_0^*, 0, 0, 1 - I_0^*).$$

(i₂) Case $\beta_{00} > 0$ and $\beta_{01} = 0$: second equation leads to $S^* = \pi_0/\beta_{00}$ and last equation to $R^* = \pi_0I_0^*/\chi$. Therefore, the equilibrium under this assumptions is

$$(S^*, I_0^*, I_1^*, R^*, D^*) = \left(\frac{\pi_0}{\beta_{00}}, I_0^*, 0, \frac{\pi_0}{\chi}I_0^*, 1 - \frac{\pi_0}{\beta_{00}} - I_0^* \left(1 + \frac{\pi_0}{\chi} \right) \right),$$

with $0 < I_0^* \leq (1 - \pi_0/\beta_{00})/(1 + \pi_0/\chi)$ to keep all species between 0 to 1. Notice that the condition $\beta_{00} > 0$ implies an incompatibility with the microscopic state $QS_{\text{mic}}^{(1)}$, as it requires $v_0^* = 0$.

(i₃) Case $\beta_{00} > 0$ and $\beta_{01} > 0$: to accomplish third equation $S^* = 0$ is required. Substituting this into first and second equation is trivial to see that $R = 0$ and π_0 are needed. With this, the equilibrium reads as:

$$(S^*, I_0^*, I_1^*, R^*, D^*) = (0, I_0^*, 0, 0, 1 - I_0^*).$$

Again, the condition $\beta_{00} > 0$ excludes the possibility of having $QS_{\text{mic}}^{(1)}$ as the micro state at equilibrium.

(i₄) Case $\beta_{00} = 0$ and $\beta_{01} = 0$: second equation implies $\pi_0 = 0$, fourth equation $R^* = 0$ and the other two equation are satisfied no matter the values of S and I_0^* . Thus, the equilibrium under this condition is

$$(S, I_0^*, I_1^*, R^*, D) = (S, I_0^*, 0, 0, D),$$

with S , I_0^* and D such that $S + I_0^* + D = 1$.

(ii) Case $\chi = 0$: equations (A2)-(A4) simplify to

$$(\beta_{00} + \beta_{01})I_0^*S = 0, \quad (\beta_{00}S - \pi_0)I_0^* = 0, \quad \beta_{01}I_0^*S = 0, \quad \pi_0I_0^* = 0.$$

Taking into account that $I_0^* > 0$ it follows that $\pi_0 = 0$ and the latter system reduces to the following three equations:

$$(\beta_{00} + \beta_{01})S = 0, \quad \beta_{00}S = 0, \quad \beta_{01}S = 0.$$

Regarding at first equation it suffices β_{00} and/or β_{01} different from zero for the condition $S^* = 0$ to hold. Otherwise, this is $\beta_{00} = \beta_{01} = 0$, S remains arbitrary. The solutions of these two possible scenarios are:

(ii₁-ii₃) Case $\beta_{00} > 0$ and/or $\beta_{01} > 0$:

$$(S^*, I_0^*, I_1^*, R, D) = (0, I_0^*, 0, R, D),$$

with I_0^* , R and D such that $I_0^* + R + D = 1$. Again, the condition $\beta_{00} > 0$, cases (ii₂) and (ii₃), implies an incompatibility with the microscopic state $QS_{\text{mic}}^{(1)}$.

(ii₄) Case $\beta_{00} = \beta_{01} = 0$:

$$(S, I_0^*, I_1^*, R, D) = (S, I_0^*, 0, R, D),$$

with S , I_0^* , R and D such that $S + I_0^* + R + D = 1$.

□

A.5 Proof of Proposition 4 (CSE)

From the assumption $I_0^* \neq 0, I_1^* \neq 0$ and (11) it follows that, necessarily, $\delta_0 = \delta_1 = 0$. That is, both master and mutant variants do not induce mortality. Moreover $0 < \nu^* = \nu(I_0^*, I_1^*) < 1$ so, in particular, the equilibrium point for the microscopic system is given by Lemma 1, that is:

$$\begin{aligned} \text{QS}_{\text{mic}}^{(\mu_c^*)} : \quad (g_0^*, g_1^*; v_0^*, v_1^*) &= \left(1 - \frac{\mu}{\mu_c^*}, \frac{\mu}{\mu_c^*}; \frac{\xi_0}{\gamma_0} g_0^*, \frac{\xi_1}{\gamma_1} g_1^*\right) && \text{if } 0 < \mu < \mu_c^* \\ &= \left(0, 1; 0, \frac{\xi_1}{\gamma_1}\right) && \text{if } \mu_c^* \leq \mu \leq 1, \end{aligned}$$

where the critical mutation probability associated to (I_0^*, I_1^*) is defined as

$$\mu_c^* = 1 - \frac{f_1}{f_0} \left(\frac{1}{\nu^*} - 1 \right).$$

We study the possible equilibria for the macroscopic system. Like in the precedent proofs, we distinguish two cases, according to the common waning immunity rate: (i) $\chi > 0$; (ii) $\chi = 0$.

(i) Case $\chi > 0$.

The macro equilibrium points come from the solutions of

$$(\beta_{00}I_0^* + \beta_{01}I_0^* + \beta_{11}I_1^*)S = \chi R, \quad \beta_{00}S = \pi_0, \quad (\beta_{01}I_0^* + \beta_{11}I_1^*)S = \pi_1I_1^*, \quad \pi_0I_0^* + \pi_1I_1^* = \chi R, \quad (\text{A5})$$

where we have taken into account that $I_1^* > 0$. Let us now consider two cases:

(i₁) Case $\beta_{00} = 0$.

From the second expression in (A5), it follows that $\pi_0 = 0$, and from the fourth one:

$$R^* = \frac{\pi_1}{\chi} I_1^*.$$

In order to get S , notice that either both $\beta_{01}, \beta_{11} > 0$ or $\beta_{01} = \beta_{11} = 0$. This is clear from the fact that $0 < \nu^* < 1$ and, hence, $\beta_{01} = 0 \Leftrightarrow (a_1 = 0 \text{ or } v_1 = 0) \Leftrightarrow \beta_{11} = 0$. Therefore, two cases arise:

(a) Case $\beta_{01} > 0, \beta_{11} > 0$.

From equations (A5) one gets:

$$S^* = \frac{\pi_1 I_1^*}{\beta_{01} I_0^* + \beta_{11} I_1^*}.$$

Thus, the complete equilibrium point is of the form

$$(S^*, I_0^*, I_1^*, R^*, D^*) \times (g_0^*, g_1^*; v_0^*, v_1^*) = \left(\frac{\pi_1 I_1^*}{\beta_{01}^* I_0^* + \beta_{11}^* I_1^*}, I_0^*, I_1^*, \frac{\pi_1}{\chi} I_1^*, D^* \right) \times \text{QS}_{\text{mic}}^{(\mu_c^*)},$$

provided that $S^* + I_0^* + I_1^* + R^* + D^* = 1$.

(b) Case $\beta_{01} = \beta_{11} = 0$.

Having in mind the third equation in (A5), we get that $\pi_1 = 0$ and so $R^* = 0$. There is no constraint for S . This means that the macroscopic system equilibrium points are given by $(S, I_0^*, I_1^*, 0, D)$ provided that $S + I_0^* + I_1^* + D = 1$. Concerning the restrictions that $\beta_{01} = \beta_{11} = 0$ imposes on the microscopic equilibrium point $\text{QS}_{\text{mic}}^{(\mu_c^*)}$, we have that they come from the fact that $\beta_{01} = \beta_{11} = 0 \Leftrightarrow a_1 = 0$ (and then, $\beta_{01} \equiv 0, \beta_{11} \equiv 0$) or $v_1^* = 0$ (which in our case is only possible if $\xi_1 = 0$ or in the limit case $\mu = 0$, not included in $\text{QS}_{\text{mic}}^{(\mu_c^*)}$). That is, the complete equilibrium points are of the form

$$(S, I_0^*, I_1^*, R^*, D) \times (g_0^*, g_1^*; v_0^*, v_1^*) = (S, I_0^*, I_1^*, 0, D) \times \text{QS}_{\text{mic}}^{(\mu_c^*)},$$

with arbitrary S, D such that $S + I_0^* + I_1^* + D = 1$ and provided $\text{QS}_{\text{mic}}^{(\mu_c^*)}$ satisfies $\beta_{01}^* = \beta_{11}^* = 0$.

(i₂) Case $\beta_{00} > 0$.

From (A5) it turns out that

$$S^* = \frac{\pi_0}{\beta_{00}}.$$

Substituting this value into the third equation in (A5), we have

$$\frac{\beta_{01}\pi_0}{\beta_{00}}I_0^* + \frac{\beta_{11}}{\beta_{00}}\pi_0I_1^* = \pi_1I_1^*$$

and, therefore,

$$I_1^* = \frac{\beta_{01}\pi_0}{\beta_{00}\pi_1 - \beta_{11}\pi_0} I_0^*, \quad (\text{A6})$$

provided that

$$\pi_1 > \frac{\beta_{11}}{\beta_{00}}\pi_0.$$

Since $I_1^* > 0$, expression (A6) implies that $\beta_{01} > 0$ and, consequently, $\beta_{11} > 0$, where we have taken into account the assertion in case (i₁) above. Finally, substituting (A6) into the fourth equation in (A5), we obtain

$$R^* = \frac{1}{\chi} \left(\pi_0 + \pi_1 \frac{\beta_{01}\pi_0}{\beta_{00}\pi_1 - \beta_{11}\pi_0} \right) I_0^*.$$

Thus, the complete equilibrium point is of the form

$$(S^*, I_0^*, I_1^*, R^*, D^*) \times (g_0^*, g_1^*; v_0^*, v_1^*) = \\ \left(\frac{\pi_0}{\beta_{00}^*}, I_0^*, \frac{\beta_{01}^*\pi_0}{\beta_{00}^*\pi_1 - \beta_{11}^*\pi_0} I_0^*, \frac{1}{\chi} \left(\pi_0 + \pi_1 \frac{\beta_{01}^*\pi_0}{\beta_{00}^*\pi_1 - \beta_{11}^*\pi_0} \right) I_0^*, D^* \right) \times \text{QS}_{\text{mic}}^{(\mu_c^*)}$$

(ii) Case $\chi = 0$.

From equation $\pi_0I_0^* + \pi_1I_1^* = \chi R$ we get that $\pi_0 = \pi_1 = 0$ and so, the equations for the macroscopic equilibrium points become

$$(\beta_{00}I_0^* + \beta_{01}I_0^* + \beta_{11}I_1^*)S = 0, \quad \beta_{00}I_0^*S = 0, \quad (\beta_{01}I_0^* + \beta_{11}I_1^*)S = 0.$$

As before, we consider two cases:

(ii₁) Case $\beta_{00} = 0$.

As before, we distinguish two possible situations:

(a) Case $\beta_{01} > \beta_{11} > 0$.

From the equations above it follows that $S^* = 0$ and arbitrary R . Hence, the complete equilibrium point is of the form

$$(S^*, I_0^*, I_1^*, R, D) \times (g_0^*, g_1^*; v_0^*, v_1^*) = (0, I_0^*, I_1^*, R, D) \times \text{QS}_{\text{mic}}^{(\mu_c^*)},$$

with arbitrary R, D such that $I_0^* + I_1^* + R + D = 1$ and provided $\text{QS}_{\text{mic}}^{(\mu_c^*)}$ is compatible with $\beta_{00}^* = 0$.

(b) Case $\beta_{00} = \beta_{11} = 0$.

In this scenario, we have that S, R , and D are arbitrary. So, the complete equilibrium is of the form

$$(S, I_0^*, I_1^*, R, D) \times (g_0^*, g_1^*; v_0^*, v_1^*) = (S, I_0^*, I_1^*, R, D) \times \text{QS}_{\text{mic}}^{(\mu_c^*)},$$

with arbitrary S, R , and D such that $S + I_0^* + I_1^* + R + D = 1$ and provided $\text{QS}_{\text{mic}}^{(\mu_c^*)}$ is compatible with the conditions $\beta_{01}^* = \beta_{11}^* = 0$.

(ii₂) Case $\beta_{00} > 0$.

In this case, it follows that $S = 0$. So the complete equilibrium point takes the form

$$(S^*, I_0^*, I_1^*, R, D) \times (g_0^*, g_1^*; v_0^*, v_1^*) = (0, I_0^*, I_1^*, R, D) \times \text{QS}_{\text{mic}}^{(\mu_c^*)},$$

with arbitrary R , and D such that $I_0^* + I_1^* + R + D = 1$

□